

Low cost applications in astronomy, atmospheric science and communications using radio waves forward scattering from meteor trails

by

Waleed Saeed Mahgoub Elsayed Madkour

Student ID Number: [1186006]

A dissertation submitted to the
Department of Engineering,
Kochi University of Technology,
Kochi, Japan

in partial fulfillment of the requirements for the degree of
Doctor of Engineering

Assessment Committee:

Supervisor: Masa-yuki Yamamoto

Co-Supervisor: Katsushi Iwashita

Co-Supervisor: Hirokazu Kobayashi

Committee Member: Masataka Takagi

Committee Member: Hideaki Nakane

March 2017

© Waleed Madkour 2017

ABSTRACT

The forward scattering of VHF radio waves by the meteor ionized trails incorporates unique characteristics for usage in various applications. The oblique incidence of radio signals off the meteor trails enables the detection of faint meteors using low power transmitters. The relatively long duration of the forward scattered signals allows more detailed analysis of the meteor trails behavior in relation to the atmospheric conditions near the meteor altitude region. It can also be used in communication of short bursts of data between distant locations on earth. In this thesis work, the usage of the forward scattering of radio waves by the meteor ionized trails in astronomy, upper atmospheric science and communication is presented. The developed meteor observation system follows the classical forward scattering setup commonly used worldwide. A methodology using locally developed software applications and interferometry technique to track the direction of each meteor echo is described as a fundamental step towards trajectory observations and hence meteor origins determination. Through using the same setup and software, the role of the secondary mesospheric ozone layer in oxidizing the meteor ionized trails was examined through meteor echoes duration distribution analysis during two meteor showers; the Perseids and the Geminids. Preliminary observations of the indirect link between the solar cycle sun spot activity level and the meteor echo durations distribution is also presented. The observational research approach in astronomy and atmospheric science aimed at extending the capabilities of the amateur basic setups by automating the observation process through software developments. These developments could fill the wide gap between the amateur system setups and the professional ones in the amount of observational data each system can provide. The methodology along with sample observational results for each application is described in detail as a proof of concept. The sample observational results in astronomy and upper atmospheric science applications are generally in agreement with the fundamentals of meteor science. Nevertheless, more statistical analysis is still required to improve the accuracy level. In line with the observational research activities, a practical feasibility study was performed on using modern technologies such as the D-STAR amateur radio network and Android in developing a flexible meteor burst communication (MBC) system. Although no positive results were obtained, the concept still needs to be examined by higher power transmitters to compensate for the higher frequency used in the 144 MHz range. The overlaps between the three applications are highlighted throughout the thesis to emphasize the necessity of considering the various factors impacting the meteor ionized trails behavior while performing a specific research. The low cost system setups introduced can be a model for low budget institutes targeting to build a practical setup for educational as well as scientific purposes.

Acknowledgment

I am thankful to my supervisor Prof. M.-Y.Yamamoto for the exceptional support throughout this work. I am also grateful to him for believing in my abilities to achieve this despite coming from a different technical background.

I would like to thank all the current members of the Space and Earth Exploration Laboratory at Kochi University of Technology for the supportive and friendly working environment along three years. I am thankful to Mr. S.Mizumoto and Mr. H.Takamasa for their support with the MBC testing. I express my special thanks to the previous KUT graduate students who worked in the meteor research group since 2004 for founding a solid basis for this work.

I am grateful to my Co-supervisors Prof. Iwashita and Prof. Kobayashi for the valuable comments and advices throughout this work. I appreciate the support of the International Relation Division members and the administrative staff in KUT for facilitating any admin work promptly.

Finally, I am grateful and indebted to my parents for their nonstop support since Kindergarten until Doctorate degree, and for encouraging me to challenge this new experience.

الحمد لله عدد أحجار النيازك في الفضاء.

“A good carpenter never blames his tools”

Table of Contents

Abstract	1
Acknowledgement	2
Chapter 1: Introduction	9
1.1 History	9
1.2 Meteor Origins.....	11
1.3 Benefits of meteors study	12
1.4 Meteor research at KUT	13
1.5 Objectives and plan.....	14
1.6 Dissertation outline.....	15
Chapter 2: Astronomical Applications	17
2.1 Introduction.....	17
2.2 Methodology	17
2.2.1 Transmitter	18
2.2.2 Receiver	18
2.2.3 Operating software	21
2.2.4 Calibration	22
2.3 Selected observations	25
2.4 Evaluation and discussion	25
2.5 Summary	29
Chapter 3: Atmospheric Science Applications	30
3.1 Introduction.....	30
3.2 Methodology	31
3.2.1 Duration measurement	31
3.2.2 Ozone concentration observation	32
3.2.3 Height estimation.....	33
3.3 Results and Discussion	34
3.4 Summary	39
Chapter 4: Meteor Burst Communication (MBC)	40
4.1 Introduction.....	40
4.2 Motivation	40
4.3 D-STAR for MBC	41
4.3.1 D-STAR operation.....	41
4.3.2 MBC connectivity	42
4.3.3 Frequency	45

4.3.4 Burst size	47
4.3.5 Capacity	49
4.3.6 Modulation	50
4.3.7 Reliability	50
4.4 Experimental setup	50
4.4.1 Transmitter	51
4.4.2 Receiver	53
4.5 Testing	54
4.5.1 Geminids 2016	55
4.5.2 Quadrantids 2017	56
4.6 Summary	56
Chapter 5: Conclusion and Future Work	58
5.1 Summary	58
5.2 Applications overlaps	58
5.3 Future work	59
5.4 Conclusion	60
Bibliography	61
Appendix A	65
Appendix B	68

List of Figures

Figure 1.1 The ancient Chinese observations of different cometary forms with mentions to various diseases and disasters associated with them around 300 B.C. (Credit: NASA/JPL).	10
Figure 1.2 An old painting depicting the Leonids meteor shower in 1833 (Credit: Elsevier/M. Littmann).	10
Figure 1.3 Diurnal variation in the arrival rate of meteors due to the Earth's orientation while orbiting the Sun.....	12
Figure 1.4 Meteors observation by forward scattering (Credit: International Meteor Organization)...	13
Figure 1.5 1033 participants of all 35 conferences coming from 50 nations with percentages of top participators. (Credit: IMC Proceedings 2016)	15
Figure 2.1 Transmitter location at Fukui (35°56'14.4" N, 136°10'18.9" E) and meteor radar location at Kochi University of Technology (33°37'16.5" N, 133°43'11.7" E).	18
Figure. 2.2 Antenna configuration of the KUT interferometer	19
Figure 2.3 Interferometry principle.	19
Figure 2.4 Relationship between observed phase shift and derived angle of arrival for cases of (a) difference in spacing: 0.5λ and (b) total spacing: 2.5λ (Figure 2.2). Shaded areas indicate the error range in phase observation and in the angle of arrival estimation.	20
Figure 2.5 Block diagram of the 5 channel receiver.....	21
Figure 2.6 Azimuth and elevation angles determination by the interferometer (Unit vectors).	22
Figure 2.7 HRO_IF_VIEW graphical results for the interferometric observation corresponding to the meteor trail image simultaneously captured by video cameras for calibration at 03:00:10 LT on 4 January 2009. The five vertical panels from up to down are: (a) Elevation angle, (b) Azimuth, (c) Phase difference for 0ch-1ch and 0ch-2ch, (d) Relative signal amplitudes of channels 0, 1, and 2, and (e) Dynamic spectrum of signal amplitude	24
Figure 2.8 Error distribution for azimuth and elevation angles measurements in Tables A.1 and A.2. The square represents 10 degrees error range.	26
Figure 2.9 Error distribution for azimuth and elevation angles measurements for meteor echoes with duration more than 3 seconds and maximum intensity level (12)	26
Figure 2.10 Error range distribution for the observational samples in Tables A.1 and A.2. The horizontal axis represents the error range in 10 degree steps for the maximum error among the azimuth or elevation angle measurements. The vertical axis represents the frequency of occurrence within the error ranges. The percentages are for the frequency of occurrence within 10 degrees error for each category.	27
Figure 2.11 The same as in Fig. 2.7 of 'HRO_IF_VIEW' graphical output, but for the four mismatched cases with durations more than 3 seconds and maximum intensity level of 12. For the top two panels of azimuth and elevation angles, the plotted data show inconsistent scattered characteristics for cases of (1), (3) and (4). For case (2), azimuth and elevation measurements are consistent but the determined elevation was different from the optical observation.	28
Fig. 3.1 Examples of meteor echoes by underdense (up) and overdense (down) trails observed by the HRO-IF-VIEW software	30

Figure. 3.2 Output images of MEC showing the duration above the overdense meteor echoes detected	32
Figure 3.3 Meteor trails height estimation by direction finding	34
Figure 3.4 The duration distribution of the Perseids overdense meteor echoes from 2005 to 2015	35
Figure 3.5 The duration distribution of the Geminids overdense meteor echoes from 2005 to 2015 ..	35
Figure 3.6 Heights of Perseids and Geminids meteor echo samples at the knee in vertical axis versus the propagation path distance ‘L’ in the horizontal axis. The horizontal dashed lines represent the average meteor height region (80–110 km). The vertical dashed lines represent the used range in the height estimation example.	36
Figure 3.7 Vertical ozone concentration profile (in cm^{-3}) calculated using the knee curves of Perseids (in blue) and Geminids (in green) by (5) and (6) compared to the SABER satellite measurements averaged over all seasons from January 2002–July 2012 (after [33]). The height ranges corresponds to the selected range of ‘L’ from 75 km to 80 km	37
Figure 3.8 Solar sunspot progression of the current solar cycle activity since 2000 (NOAA/SWPC). Marks with red show the points of comparison	38
Figure 3.9 The duration distributions of the Geminids 2006 (minimum solar activity) and Geminids 2011 (maximum solar activity)	38
Figure 4.1: Communication options through the D-STAR network	42
Figure 4.2: Cellular networks coverage in the Saharan desert (Credit: coveragemaps.com).....	43
Figure 4.3 Cellular coverage in Egypt (Credit: Etisalat Egypt).	44
Figure 4.4 D-STAR repeaters in southern Europe (Credit: dstarinfo.com)..	44
Figure 4.5 The nearest D-STAR C-Band Gateway Repeater in Cyprus with theoretical MBC coverage area of ~2200km.....	45
Figure 4.6 Geometry of radio signals forward scattering by meteor trails	46
Figure 4.7 Scattered signal relative amplitude in relation to the used frequency.....	47
Figure 4.8 The DV frame structure	48
Figure 4.9 Time domain signal of an SOS message transmitted by the Android RS-MS1A application in the DV mode.	48
Figure 4.10 The meteor scattering duration by underdense trails in relation to the frequency used ...	49
Figure 4.11 Increasing the capacity of MBC system through Bluetooth pairing	49
Figure 4.12 Experimental setup.....	52
Figure 4.13 The MBC box.....	52
Figure 4.14 The developed MBC Test application and the ICOM RS-MS1A.	53
Figure 4.15 SOS message received by the D-RATS software.....	54
Figure 4.16 SOS message raw data received by the serial monitoring software.....	54

Figure 4.17 Initial testing location during the Geminids meteor shower.....	55
Figure 4.18 Meteor trail locations and the corresponding illuminated ground footprints... ..	56

List of Tables

Table 2.1 Calibration results derived from comparison with optical observation by video cameras	23
Table 4.1 Mobile transmitter specifications	53
Table 5.1 Overlapping parameters among the three applications.	59
Table A.1 Simultaneous observation results by the interferometer (shaded rows) and video cameras (white rows) for the north-west direction (first camera FOV)	65
Table A.2 Simultaneous observation results by the interferometer (shaded rows) and video camera (white rows) for the south-east direction (second camera FOV).....	67

CHAPTER 1

Introduction

1.1 History

The illuminating objects randomly seen falling in the sky during clear nights and commonly known as “shooting stars” are always of great interest to common people as well as to professional scientists. The majority of people are now aware that these shooting stars are in fact meteoric objects entering the Earth’s atmosphere during its orbit around the sun. These visual strikes of large meteors constitute a small portion of millions of meteoric dust particles swept by the Earth daily. The majority of the meteoric objects known as “meteors” entering the atmosphere at high speeds ranging from 12-72 km/s are burned by collisions with the atmospheric particles forming heat, light and ionized trails. Other few meteoric objects known as “meteorites” survive their way through the atmosphere until they hit the Earth’s ground.

The interest in observing meteoroids (the particle in space before being a meteor or meteorite) is extended back to ancient history where several archaeological remains marked falling stars in different locations on Earth. A common belief among ancient observers has linked the meteoroids appearance to bad omens such as diseases, disasters or deaths. The Chinese ancient observations back to ~300 B.C. are one of the clearest examples that showed coincidence with the Halley comet’s appearance times calculated later (Fig. 1.1). A comprehensive historical record of visual observations of meteor showers over 25 centuries from China, Japan and Korea were translated and published in [1]. Records from the ancient Egyptian history also show that meteorites were used in the making of iron tools [2]. The meteoroids phenomena remained mysterious until the recent history in the 19th century, particularly in 1833 when the people in the east of the United States have noticed hundreds of meteors coming from the same direction in the sky (Fig. 1.2). The incident has drawn the Astronomers attention at that time and after extensive research the astronomer Denison Olmsted concluded that these meteors are originating from deep space [3]. The wheel of the meteors research started spinning since then and the phenomena of meteor showers was confirmed; at certain times of the year a stream of meteors originating from the same point in the sky is regularly observed. Soon after, the connection of meteor showers origin to comets was demonstrated by Giovanni Schiaparelli in 1861 [4]. The popular meteor shower incident in 1833 was realized after then to be the Leonids meteor shower originating from the trail of the periodic comet 55P/Tempel-Tuttle. The meteor research in the 19th century moved through slight improvements after then relying on visual observation recordings by comparing the meteor detected positions to the star charts. Meteor counts, magnitudes and originating directions in the sky (Radiant points) were the main parameters observed and annual charts started to be generated. These visual records although missed the accuracy required to discover deeper facts about the meteors, it has kept the wheel of meteor research spinning until the developments of the modern techniques of meteor observation has started in the 20th century.



Figure 1.1 The ancient Chinese observations of different cometary forms with mentions to various diseases and disasters associated with them around 300 B.C. (Credit: NASA/JPL).



Figure 1.2 An old painting depicting the Leonids meteor shower in 1833 (Credit: Elsevier/M. Littmann).

In the early 20th century, the developments in the optical observation tools have dramatically improved the meteor scientific research. Telescopes, multi-station cameras and photoelectric observations have extended the limited detection ability of visual observations and thus allowed more accurate observations on meteor flux rates, velocities and origins (*e.g.* [5, 6]). The optical and visual observation methods although are still playing a major role in the meteor scientific research till now, they are limited by the risk of discontinuity. These tools become completely blind in the daytime and during cloudy nights which causes many meteoric events to go unobserved. The need for a supportive reliable and continuous observation method has raised the potential of using radio signals in meteor observations.

The remarkable beginning of radio observations was led by Breit and Tuve in the United States in 1926 who studied the reflection of radio waves from the upper atmospheric ionized layers [7]. Three years later, the Japanese physicist Hantaro Nagaoka suggested a direct relation between meteors and the scattered radio waves of unknown source [8]. Thereafter, several radio researchers worldwide have noticed the increased radio reception activity during meteor showers until it was confirmed in 1944 during world war II that the source of the received radio signals are not only from missiles but also from meteor ionized trails. The bright meteors above England have caused a lot of false warnings when forward scattered radio signals by meteor trails are detected by the defensive radars. Meanwhile by the end of the war, the role of the meteor trails in scattering these unknown-source signals was recognized and several military radars were converted to scientific meteor observation radars. At this point, the interest in meteor science has grown worldwide and many groups were formed using combined optical and radio systems. These systems varied widely in their techniques and objectives but generally stayed in the same category of being ground-based observation tools. The rapid developments in the field of space crafts and orbiting satellites in the late 20th - early 21st century have added another dimension from space to meteor observations. One of the targets of the most recent proposed Extreme Universe Space Observatory on board the Japanese Experiment Module (JEM-EUSO) of the International Space Station (ISS) is to provide a wider coverage of meteors detectability [9].

The history of meteor research by each observation instrument is very rich and can constitute a separate thesis. Interested readers can refer to several books and articles that comprehensively describe the step-by-step evolution of meteor observation tools (*e.g.* [10, 11 and 12]).

1.2 Meteor origins

Meteors are classified into two categories according to their originating source; the shower meteors originating from the debris of orbiting comets crossing by the Earth's orbit, and the sporadic meteors of various origins from the solar system planetary dust such as the asteroid belt (*e.g.* [13]). Each regular meteor shower such as the Geminids, Perseids or Leonids has almost a predefined calendar date every year with slight changes in the range of hours. The characteristics of these regular showers are well studied and the shower parameters such as radiant, velocity, flux, and mass distributions are regularly observed and recorded worldwide. Other non-periodic meteor showers occasionally occur resulting from comets passing nearby the Earth's orbit once every very long time periods such as the Camelopardalis meteor shower in 2014 originating from the parent comet 209P/LINEAR discovered in 2004. Sporadic meteors constitute around 80% on average of the total observed meteors with varying diurnal and

seasonal arrival rates. The diurnal variations is due to the orientation of the Earth while it orbits the Sun (Fig. 1.3). The peak flux rate happens during the hours around the sunrise time when the Earth's front is sweeping meteors and the minimum at the sunset time when few meteors overtake the Earth's rear. Seasonal variations also exist with a maximum flux rate during summer and a minimum during winter (e.g. [14]).

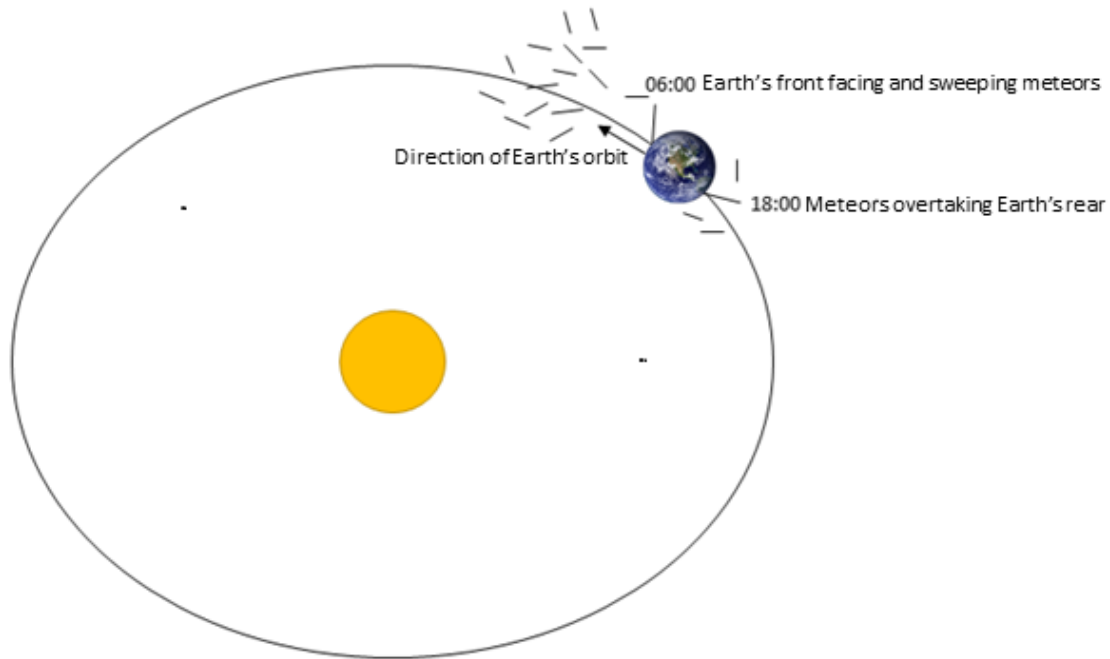


Figure 1.3 Diurnal variation in the arrival rate of meteors due to the Earth's orientation while orbiting the Sun.

1.3 Benefits of meteor study

The characteristics of the meteoric particles originating from the deep space can be a rich source of information on various research areas. The analysis of the age and composition of the dust particle elements can be one of the clues that reveal information on the solar system evolution. The behavior of the meteoroids during its entry to the Earth's atmosphere at high speeds and its friction with the atmospheric molecules reflects the changing atmospheric conditions at the meteors altitude region of 70 - 120 km. As several satellite missions were severely impacted by meteoric particles such as the failed mission of NASA Landsat-5 imaging satellite during the Perseids meteor shower in July 2009, anticipating meteor flux rates becomes an essential step while selecting the location and time for launching spacecrafts [15]. Moreover, the meteor ionized trails ability to forward scatter radio signals has introduced a natural communication medium for transferring short bursts of data between two distant points on Earth. A more comprehensive insight into the current meteor research activities worldwide can be found in the Meteoroid 2016 conference website [16]. The wide research areas of meteor studies through different instruments and techniques has triggered the foundation of a meteor research group at KUT by graduate students.

1.4 Meteor research at KUT

As the meteor research group was initiated by graduate students from the engineering department at KUT, developing ground-based radio observation instruments was the main objective. As previously mentioned, ground-based radio observation has the advantage of continuity irrespective of weather conditions. Also, the detectability of meteors at low altitude levels might be more efficient from ground than from space-based satellites. Ground meteor radio observation systems are designed following backscattering or forward scattering techniques. In the backscattering systems, radio waves from the transmitter hit the meteor trails at a right angle and are reflected back towards a receiver collocated with the transmitter location. The backscattering geometry is simple and facilitates the observation process of various meteor parameters such as the meteor height and velocity. The majority of the professional observation systems are of the backscattering type. High-power large-aperture (HPLA) radars are used by high budget institutes such as the monostatic Middle Atmosphere Alomar Radar System (MAARSY) in Norway or the Middle and Upper Atmosphere radar (MU radar) in Japan. In the forward scattering systems, radio waves from the transmitter hit the meteor trail at an oblique incidence angle. The scattered signal is then forwarded to a distant location depending on the orientation of the meteor trail (Fig. 1.4). The geometry of the forward scattering systems is more complex than that of the backscattering ones. However, the forward scattering feature unique advantages over the backscattering: 1- The longer duration of scattered signals due to oblique incidence enables the detection of fainter meteors and a more detailed observation of the meteor ionized trails behavior. 2- The possibility to communicate over long distances through short signal bursts and 3- The possibility of constructing passive radars to receive meteor echoes scattered from various VHF sources such as the TV or radio broadcasting stations.

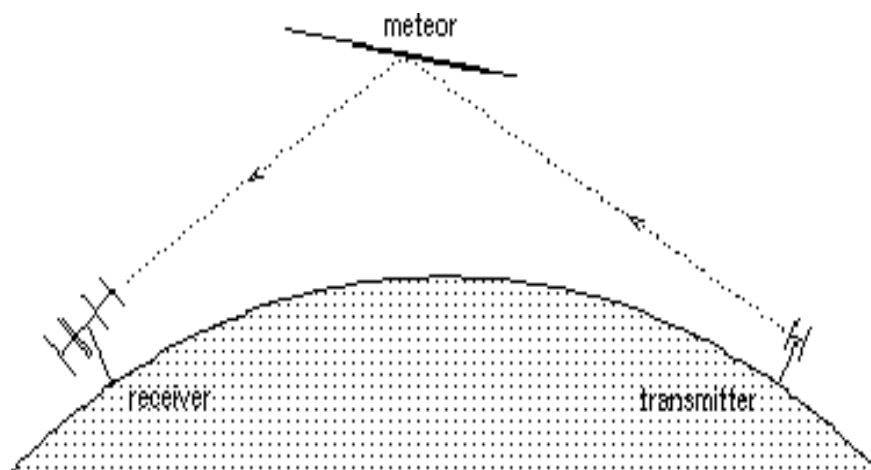


Figure 1.4 Meteors observation by forward scattering (Credit: International Meteor Organization).

Initially, the meteor research started at KUT through optical observation activities among the Meteor Train Observation (METRO) campaign during 1998-2002. The METRO campaign relied on photographic and video images of amateur observers in Japan to collect 439 images of persistent meteor trains of the Leonids meteor shower [17]. The evolution of the meteor

Ham-band Radio Observation (HRO) in Japan started in April 1996 by the setup of a 50 W continuous wave beacon signal at 53.75 MHz transmitted from the Fukui National College of Technology (FNCT) at Sabae, Fukui prefecture [18]. The KUT radio observation development started in 2004 following the classical setup of the forward scattering systems as described by the International Meteor Organization (IMO). The basic system was constructed in a 3-channel interferometric configuration to receive the forward scattered radio signals generated from the Sabae station. The system applied interferometry principles to detect the meteor echo directions before it was upgraded to 5 channels in 2007 to enhance the direction finding accuracy. To improve the observation process, a set of software applications was developed in 2008 to automate counting of meteor echoes, filtering noise, measurement of meteor echo durations, and meteor direction finding. Optical observation by video cameras was also used in parallel to calibrate the radio measurements and test the interferometer accuracy. In 2009, a calibration device was developed to calculate the absolute reception power and estimate the meteor trails density. In 2012, two additional remote receiving stations were constructed at approximately 15 km far from the interferometer location at KUT to enable observing meteor trajectories and velocities. Due to the absence of graduate students working on the subject, the system stopped working from April 2012 until the start of this thesis work on April 2014.

1.5 Objectives and plan

The initial objective of this thesis work was to quickly revert the system into its last status in 2012 and achieve a stable automated observation process. The new team comprised two graduate students in masters and doctor course (this thesis). The next objective was to maximize the usage of the basic forward scattering system in various applications. Previously, the entire work performed at KUT was devoted to the astronomical research. Several software applications were developed to reach an automated continuous observation process of astronomical parameters with an acceptable accuracy. The plan was to invest in the available automated process in acquiring large amount of data that can be suitable for astronomical as well as upper atmospheric science analysis. After gaining adequate experience with the techniques of forward scattering by meteor ionized trails, the meteor burst communication (MBC) appeared to be a practical engineering application for the scientific background. The meteor research plan at KUT was then branched into three parallel research themes: 1- Astronomy, 2- Atmospheric science, and 3- Communication. Due to the limited time available, the internal objective at KUT was to provide a proof of concept for each application methodology that can enable a wider research opportunities for the next students in the future.

The positioning of the KUT meteor observation system as a basic low cost system in relation to the international meteor research community was another objective. Although the developments in the meteor research has grown rapidly worldwide in the last decades, the advanced level research community remained very narrow. A clear indication of this is the chart summarizing the participation per country in the international meteor conference (IMC) - the top conference for meteor amateur work- along 35 years (Fig. 1.5). The majority of participation is normally from the European countries as the conference is usually held in Europe. The remaining is concentrated in the developed countries of USA, Australia and Eastern Asia, with negligible participation from other regions (Africa, Latin America, and Middle East). The community becomes even narrower as we look at the participation in the top professional level conference “Meteoroids 2016” held at the European Space Agency (ESA)

[16]. Not only the number of participating countries are less, but also the instruments are more advanced and the budget of the ongoing research projects is higher. Thus, a gap currently exists between the professional high cost systems and the amateur low cost instruments.

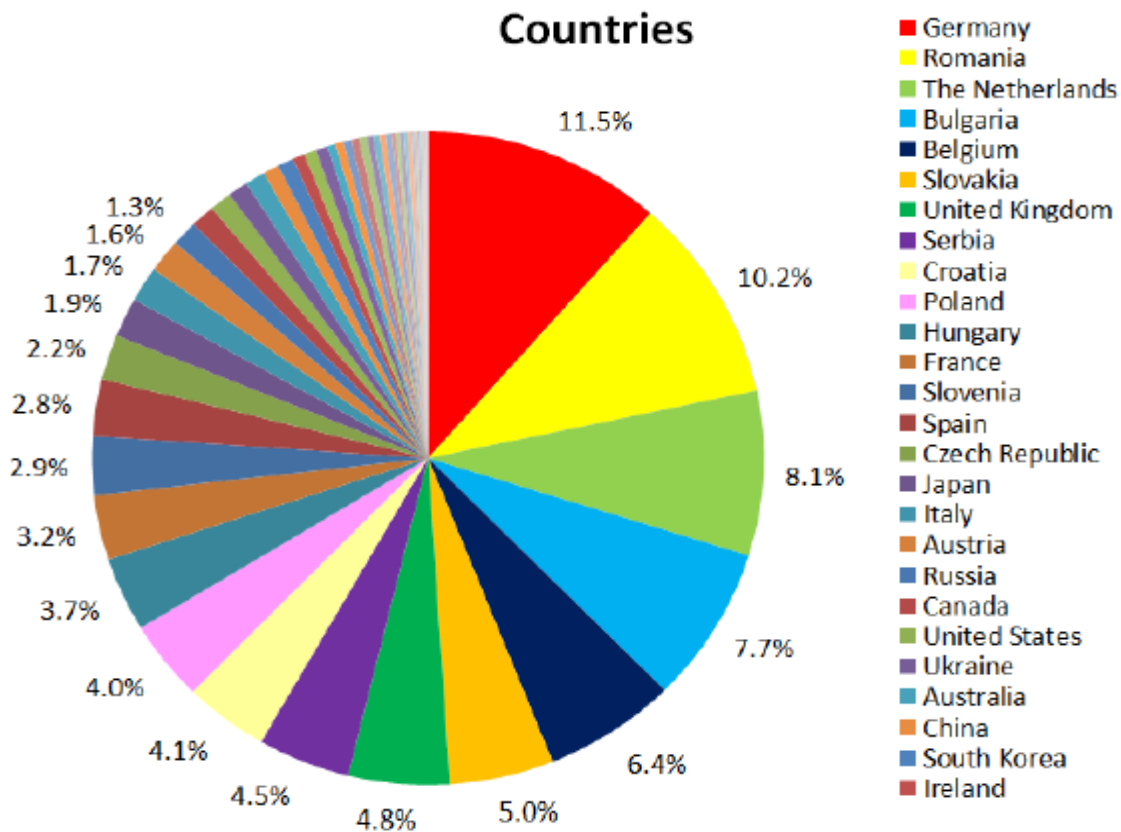


Figure 1.5 1033 participants of all 35 conferences coming from 50 nations with percentages of top participants. (Credit: IMC Proceedings 2016).

The work described in this thesis targets to play a role in filling the gap between the professional and amateur ground radio observation instrumentation. This can be achieved through improving the capabilities of the classical low cost amateur system setups by software automation of the observation process. Automation shall allow continuous observation and hence provide a sufficient amount of observational data that can be used in statistical analysis. The meteor observation system described can be replicated or customized as an ideal entry step for institutes at the developing nations into a practical space research activity.

1.6 Dissertation outline

The thesis is formed of five chapters, with a basic introduction chapter at the beginning and a general conclusion Chapter at the end. Three applications where radio forward scattering from meteor trails is used are described separately in the Chapters 2 to 4. Included in each of these chapters, a more detailed introductory section relative to the subject, a description of the

methodology and tools used, and sample results to discuss the methodology as a proof of concept. Chapter 3 describes the methodology applied for meteor direction finding by the KUT forward scattering radar. The use of the same forward scattering setup in mesospheric ozone concentration and solar cycle activity observations is described in Chapter 4. In Chapter 5, a practical study on the potential use of D-STAR (Digital Smart Technologies for Amateur-Radio) network for meteor burst communication (MBC) is explained. Despite being distinct research fields, the three applications are not sharply isolated from each other and the overlapping areas where meteor science in each crossover are highlighted. The overall evaluation of the research results is summarized in the conclusion section in Chapter 5 along with wide options and recommendations for future work.

CHAPTER 2

Astronomical Applications

2.1 Introduction

At the beginning period of this research thesis, an example of a rare meteor shower, the Camelopardalids occurred in May 2014. This meteor shower was originated from a newly discovered comet 209P/LINEAR in 2004 and therefore, it was considered as a unique opportunity to gather the maximum information possible on an old comet by observing its meteor shower parameters. Such a rare event is an example where continuous meteor radio observation provides a reliable method in astronomical observations regardless of changing weather conditions during unique events.

The orbits of a meteor shower parent comet is deduced by the analysis of the meteor shower parameters such as trajectory, velocity, and mass. A direction finding technique is necessary for the determination of these parameters. A proven method for direction finding is the phase difference detection by interferometric analysis by multi-receivers meteor radar configurations. Interferometric meteor radar systems vary in size, power, technique and cost. HPLA radar systems with tens or hundreds of arrayed antennas such as the MAARSY system in Norway use complex interferometric analysis over large number of receiving channels to detect the phase differences [19]. On the other hand, low budget educational institutes, laboratories in small universities or amateur observer groups cannot afford to build systems at this level and they tend to build alternative basic systems such as the one described in this chapter.

The forward scattering observation system, although is geometrically more complex than the backscattering system, has the advantages of lower power requirements and longer duration meteor echoes. Professional forward scattering systems usually tend to improve the reception probability by using a network of receivers (e.g. [19]). The presented system configuration at KUT follows the interferometric configuration setup explained in [20]. This configuration is common to the radio meteor observers worldwide, however, it remains a challenging task to construct a reliable algorithm to automate the continuous observation of the meteor showers parameters. In this chapter, the KUT meteor observation method for astronomical use as an example of a basic forward scattering setup is explained. The developed software structure is explained along with sample observational results of meteor echo directions compared to simultaneous video camera observations to verify the effectiveness of the methodology.

2.2 Methodology

The five channels KUT meteor observation system utilizes the forward scattering of 53.75 MHz radio signals transmitted from the Sabae station, Fukui, Japan at a distance of 340 km from Kochi (Fig. 2.1). The system comprises of three subsystems; the transmitter, the receiver and the operating software.

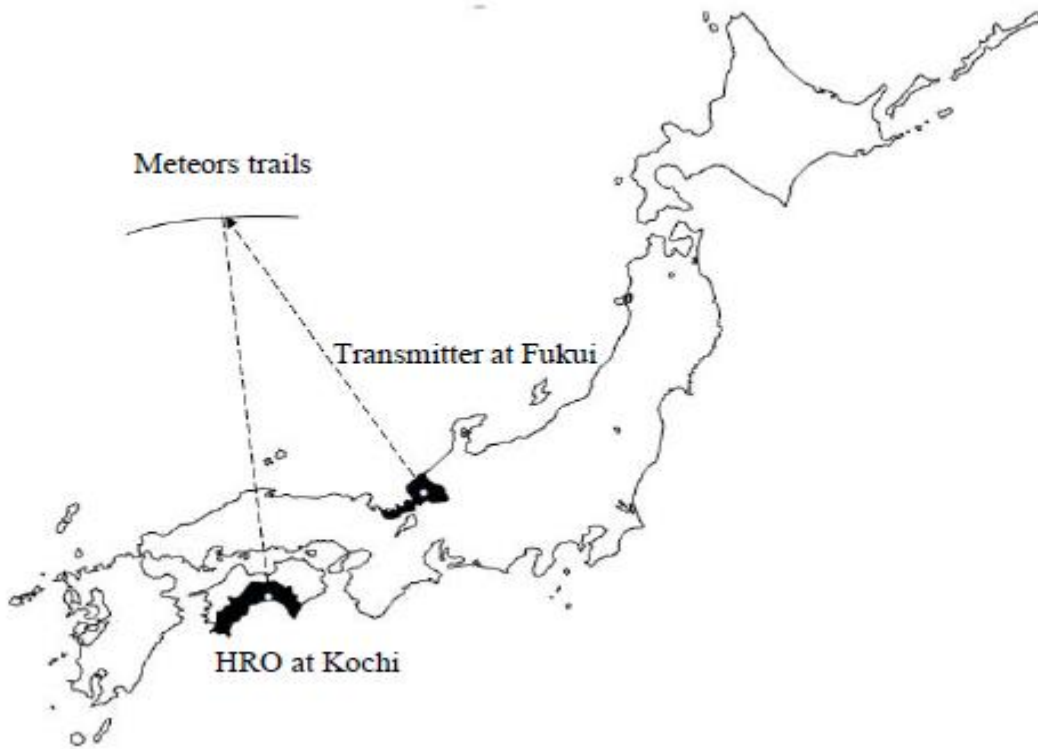


Figure 2.1 Transmitter location at Fukui (35°56'14.4" N, 136°10'18.9" E) and meteor radar location at Kochi University of Technology (33°37'16.5" N, 133°43'11.7" E).

2.2.1 Transmitter

Since 1999, a transmitter has been operated for radio meteor observation general use all over Japan. A two elements crossed Yagi antenna is used to transmit continuous wave (CW) at 50 W power and 53.75 MHz frequency from the Sabae station generated by an ICOM IC-706 transmitter. The transmitter was designed to radiate an Omni-directional pattern over a wide range of elevation with more than 70° zenith angle [18].

2.2.2 Receiver

Five two-element crossed Yagi antennas in an elongated cross pattern setup with a common central antenna are used to receive radio signals scattered from meteor ionized trails (Fig. 2.2). The antenna configuration was designed to apply the interferometry technique to incident waves in order to determine the precise direction of meteor echoes. The basic principle of interferometry is applied between any two independent antennas from the five to obtain phase differences. As shown in Fig. 2.3, the wave path difference D between received signals is directly proportional to the spacing between the two antennas d by:

$$D = d \cdot \sin \theta \dots\dots\dots (1)$$

where θ is the angle of arrival of incoming waves.

The phase shift φ depends on the path difference D as well as on wavelength λ of the observing frequency by:

$$\varphi = (2\pi D) / \lambda \dots\dots\dots (2)$$

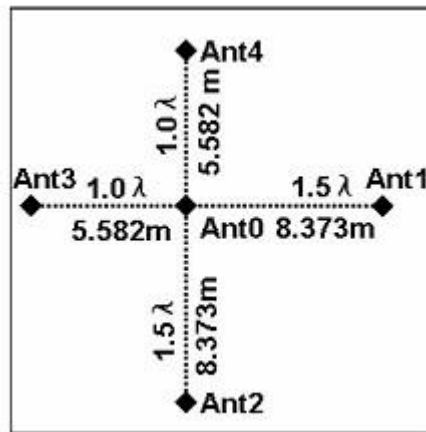


Figure 2.2 Antenna configuration of the KUT interferometer.

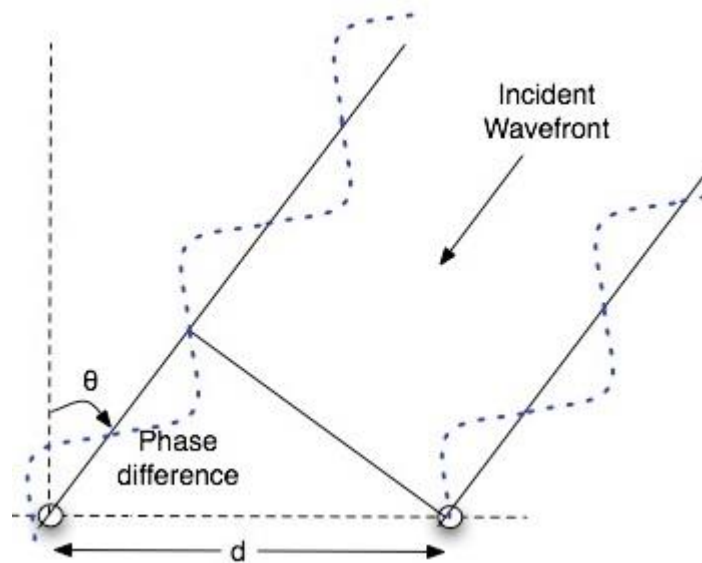


Figure 2.3 Interferometry principle.

To measure the angle of arrival accurately using the interferometer, the antenna spacing was selected as a compromise between the periodic ambiguity resulted from the use of a long spacing (multiples of 2π) and the mutual coupling resulting from the use of a short spacing (spacing less than or equal to 0.5λ). This can be optimally achieved by selecting adjacent antennas spacing meridionally or zonally so that the difference between them is equal to 0.5λ [20]. For the antennas configuration shown in Fig. 2.2, two estimates of angle of arrival exist, the first is from the difference in spacing $\text{Ant0Ant1} - \text{Ant0Ant3} = 0.5\lambda$, which gives a low accuracy single estimation with no periodic ambiguity, while the second is from the total spacing $\text{Ant0Ant1} + \text{Ant0Ant3} = 2.5\lambda$, which gives estimates with high accuracy but with

periodic ambiguity. Figure 4 represents an example of phase estimation where the single estimation in the case of a short spacing removes the ambiguity present for the long spacing.

The radio signals received by the five antennas are fed into a hardware system of five receivers, a PC with a multiple channel A/D board (SAYA, ADX85-1000), and a Garmin GPS circuit for accurate time synchronization (Fig. 2.5). The receivers are of a super-heterodyne design, where the radio frequency detected is triple down-converted to a baseband signal. For our case using a received signal of 53.75 MHz, a 43.055 MHz oscillator for the first local signal and a 10.6941 MHz one for the second are selected. The 2 local signals are mixed with the received radio signal and BFO (beat frequency oscillator) of 455 kHz to produce a 900 Hz audio output signal. Interferometric information of each meteor echo is then realized by data analysis on the PC, where an A/D board of 1 MHz sampling in total with eight analog inputs is used for five channel data acquisition from the receivers, in addition to one channel for an accurate timing signal of one PPS (pulse per second) provided by the GPS receiver. From the common local oscillators, each local signal is distributed to the five channels so as to maintain the observed phase shift into the down-converted signals.

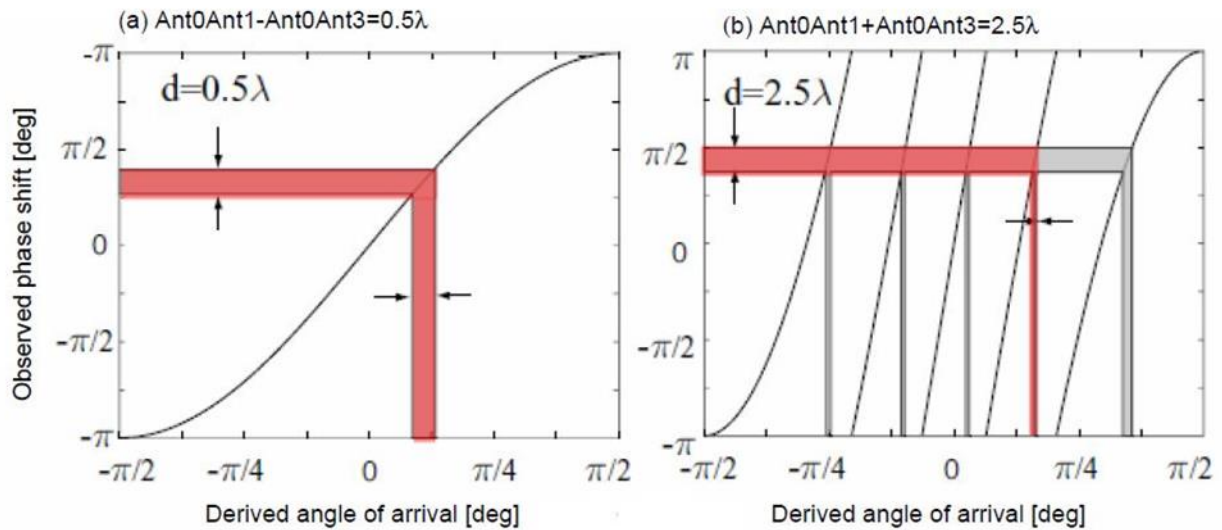


Figure 2.4 Relationship between observed phase shift and derived angle of arrival for cases of (a) difference in spacing: 0.5λ and (b) total spacing: 2.5λ (Figure 2.2). Shaded areas indicate the error range in phase observation and in the angle of arrival estimation.

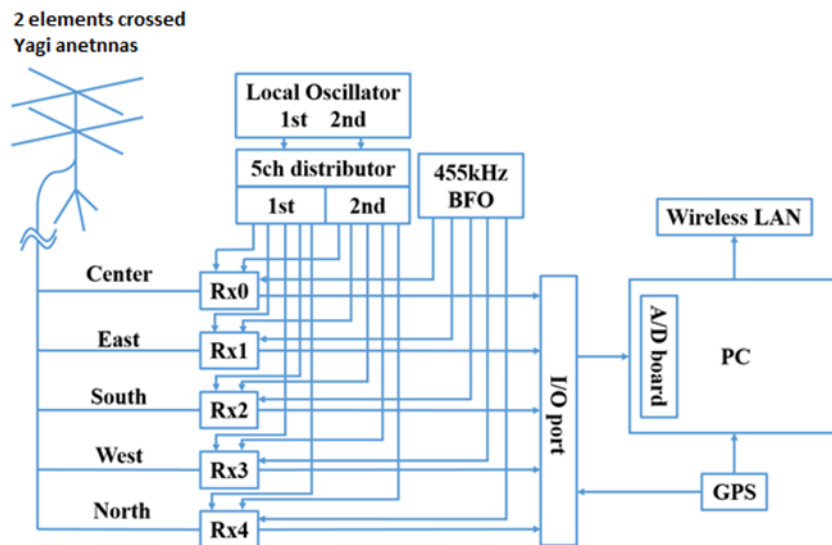


Figure 2.5 Block diagram of the 5 channel receiver.

2.2.3 Operating software

The common software used in radio meteor observations in Japan and worldwide HROFFT (Ham-band Radio meteor Observation Fast Fourier Transform) generates spectrogram images for meteor echoes in 10 minute intervals with a total of 144 images per day. As the counting of meteor echoes on the spectrograms manually is not considered a standard method and consumes a lot of effort and time, the software “Meteor echo counter” was developed locally at KUT in 2007 to automatically count meteors based on image processing techniques. It can also distinguish between meteor echoes and noise disturbances from other sources such as airplanes and thunderstorms [21]. The software was then upgraded in 2008 to analyze the interferometric phase differences and generate information on meteor echo directions every 10 minutes.

The operating software of the interferometer consists of three parts: (1) a sampling program for the A/D board interface to create a fixed-size swapping input file (7.5 seconds each) on a 128 MB memory drive on the PC, (2) a file combining program gathers the 7.5-s swapped files and combines them into a ten minute data file with precise referring to the 1 PPS signal for time adjustment, and (3) the data analysis software ‘HRO-IF-V2’ which calculates the phase shift between the two antennas on each of the E-W and N-S axes to deduce the 3-dimensional echo direction from the equations:

$$\text{Azimuth} : \alpha = \tan^{-1}(\cos \theta_2 / \cos \theta_1) \dots\dots\dots (3)$$

$$\text{Elevation} : \beta = \cos^{-1}(\cos \theta_2 / \cos \alpha) = \cos^{-1}(\cos \theta_1 / \sin \alpha) \dots\dots\dots (4)$$

where θ_1 and θ_2 are the angles of arrival of the incoming waves for East axis and South axis planes, respectively (Fig. 2.6).

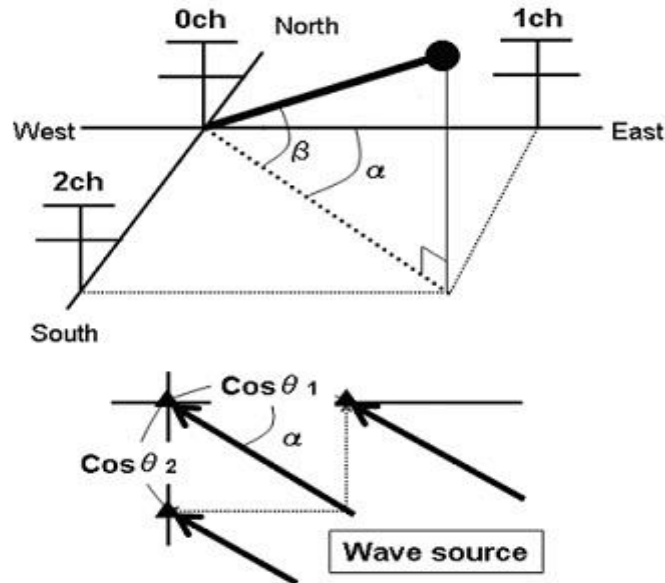


Figure 2.6 Azimuth and elevation angles determination by the interferometer (Unit vectors).

Phase spectrum analysis is performed by 'HRO-IF-V2' to obtain the direction of each meteor echo, where a dynamic spectrum is created by FFT conversion into a frequency range of 850-1050 Hz every 0.1 second in addition to the detailed intensity profiles of the five independent channels with 43.4 kHz data sampling. The outcome of phase difference analysis can then be displayed by 'HRO-IF-VIEW' software that provides a graphical interface for the interferometric data. The 'HRO-IF-VIEW' output graph shown in Fig. 2.7 consists of 5 vertical panels with a common horizontal time axis. The horizontal time axis is scaled in counts of 0.1 seconds for a maximum of 10 minute intervals (6000 counts). The meteor echo in Fig.2.7 was received during the 10 minutes interval from 3:00:00 to 3:10:00, between 100 and 250 counts after 3:00:00 (3:00:10 and 3:00:25). Vertically, The upper 2 panels display the elevation and azimuth angles, the middle panel displays the raw phase shifts between channel 0 and channel 1 (E-W axis) and between channel 0 and channel 2 (N-S axis), the real phase shift is plotted as cross marks by adding the calibration values, the fourth panel displays the relative signal amplitudes of channels 0, 1 and 2 used in phase difference determination, and lastly the bottom panel displays the amplitude dynamic spectrum in the range 850-1050 Hz divided in 20 steps, (e.g., in Fig. 2.7, the peak at 3 represents a frequency of 880 Hz).

2.2.4 Calibration

The correct output of phase shift analysis from interferometry by 'HRO-IF-V2' is the most significant stage for the observation of meteor directions. In order to achieve a correct direction determination, calibration experiments by the interferometer in comparison with optical meteor observation were carried out. Video records of bright meteors taken at an adjacent location in KUT by a high-sensitivity CCD (Charge-Coupled Device) video cameras (Watec, Neptune-100N) with field of view (FOV) of 57° x 42° were used as absolute coordinate references.

A meteor image clearly captured by the video cameras on 4 January 2009 with azimuth and elevation angles of 349.4° and 43.9°, respectively, was used for calibration. As demonstrated in Fig. 2.4, the phase differences corresponding to these values ought to provide two estimates for the 0.5λ and 2.5λ cases in each direction of E-W and N-S. Table 2.1 summarizes the calibration results that were used as a reference for interferometer observation including the intrinsic (instrumental) phase shift from the antennas to the receiver circuits. The estimated errors for a phase uncertainty of $\pm 5^\circ$ are included.

Table 2.1 Calibration results derived from comparison with optical observation by video cameras.

	0.5λ		2.5λ	
	E-W	N-S	E-W	N-S
Calibration value	- 62.5°	+ 8.5°	- 272.3°	+ 12.8°
Estimated errors for phase uncertainty of $\pm 5^\circ$	$\pm 6.1^\circ$	$\pm 6.1^\circ$	$\pm 1.2^\circ$	$\pm 1.2^\circ$

* Referring to Fig. 2.4, for each direction, two phase estimates exist for each case of 0.5λ and 2.5λ . These calibration values were configured in the 'HRO_IF_V2' software analysis to correct for intrinsic phase shifts.

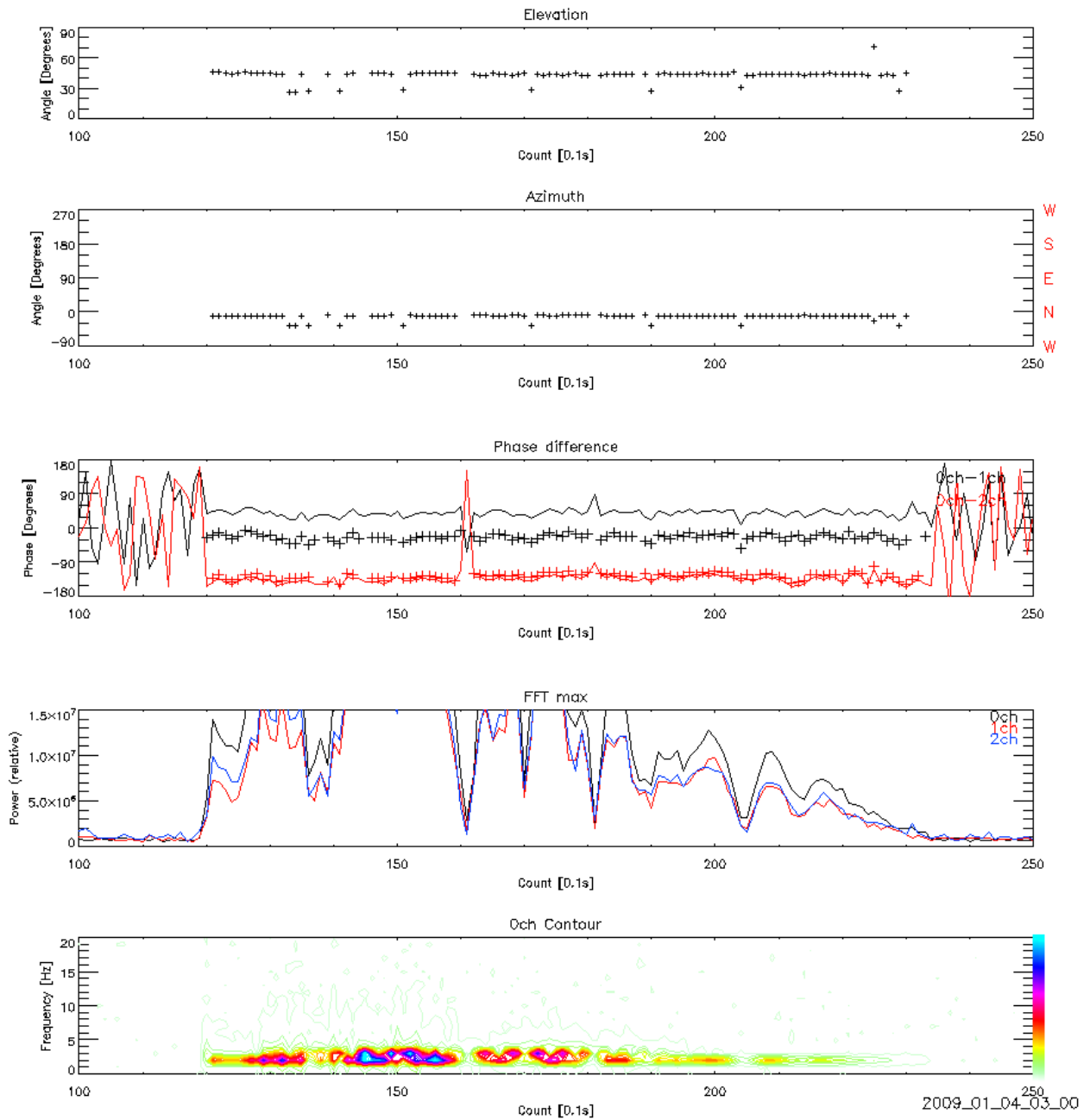


Figure 2.7 HRO_IF_VIEW graphical results for the interferometric observation corresponding to the meteor trail image simultaneously captured by video cameras for calibration at 03:00:10 LT on 4 January 2009. The five vertical panels from up to down are: (a) Elevation angle, (b) Azimuth, (c) Phase difference for 0ch-1ch and 0ch-2ch, (d) Relative signal amplitudes of channels 0, 1, and 2, and (e) Dynamic spectrum of signal amplitude.

2.3 Selected observations

The system efficiency in automatic counting of meteor echoes from HROFFT images using image processing was verified in [20]. To test the accuracy of meteor echo direction measurements, selected simultaneous measurements by the interferometer and video cameras during and after the Quadrantid meteor shower (QUA) in 2009 were compared [see Appendix A]. Optical observation was performed using two video cameras in the north-west and south-east FOV at a location 40 meters away from the interferometer. The azimuth and elevation angles radio measurements were extracted from the text files generated from the interferometric analysis performed by “HRO_IF_V2” where the calibration values in Table 2.1 were preconfigured. Duration and intensity were measured by the “Meteor Echo Counter” software where the relative intensity is graded on 13 levels (from 0 to 12) according to the power spectrum of HROFFT spectrograms, with 0 as the lowest intensity level.

Among the all 42 results obtained in the selected period, there exist 20 records for meteor echoes with duration less than or equal to 3 seconds and 22 records for meteor echoes with duration longer than 3 seconds. The classification of meteor echoes into 2 categories according to their durations is due to the significant improvement observed in system accuracy for meteor echoes with durations more than 3 seconds. The system accuracy for different categories is discussed in the next section by error analysis.

2.4 Evaluation and discussion

The duration and intensity of meteor echoes shows significant impact on the accuracy of the interferometric direction finding system. The error distribution results for the different categories are summarized in Fig. 2.10 Error analysis of the interferometer azimuth and elevation angles samples showed 55% agreement with optical observations within an error range of 10 degrees (Fig 2.8). By filtering the analysis to only echoes with the maximum intensity (level 12), the agreement level was raised to 68%. Although the intensity levels are only indicative of the relative signal strength, not the signal to noise ratio (S/N), the intensity related improvement can agree with results of similar studies if the noise level is checked on the background of HROFFT images. Meteor echoes longer than 3 seconds showed a higher agreement level of 82% within 10 degrees error and 80% for the same type of echoes but with the maximum intensity level of 12 (Fig. 2.9). This significant improvement is logically due to the long echo durations relative to the system sampling resolution of 0.1 seconds in “HRO_IF_V2” analysis which does not provide enough sampling points for shorter duration meteor echoes. On the other hand, higher intensity levels did not show a remarkable impact on the accuracy for this type of echoes.

Three of four cases in disagreement out of samples of 22 meteor echoes with durations more than 3 seconds (marked by (1), (3) and (4) at the right most column of Tables A.1 and A.2 in Appendix A) showed inconsistent azimuth and elevation records in the “HRO_IF_VIEW” graphs (Fig. 2.11). This inconsistency can possibly be due to the presence of high trees and buildings around the interferometer test site location in KUT that may cause extra signal reflections. The fourth case marked by (2) at the right most column of Table A.2 shows agreement in azimuth measurements but different elevation measurements although consistent. The event occurred during the peak flux period of Quadrantids meteor shower (QUA) and could be a result of two different meteors detected by each of video cameras and the interferometer.

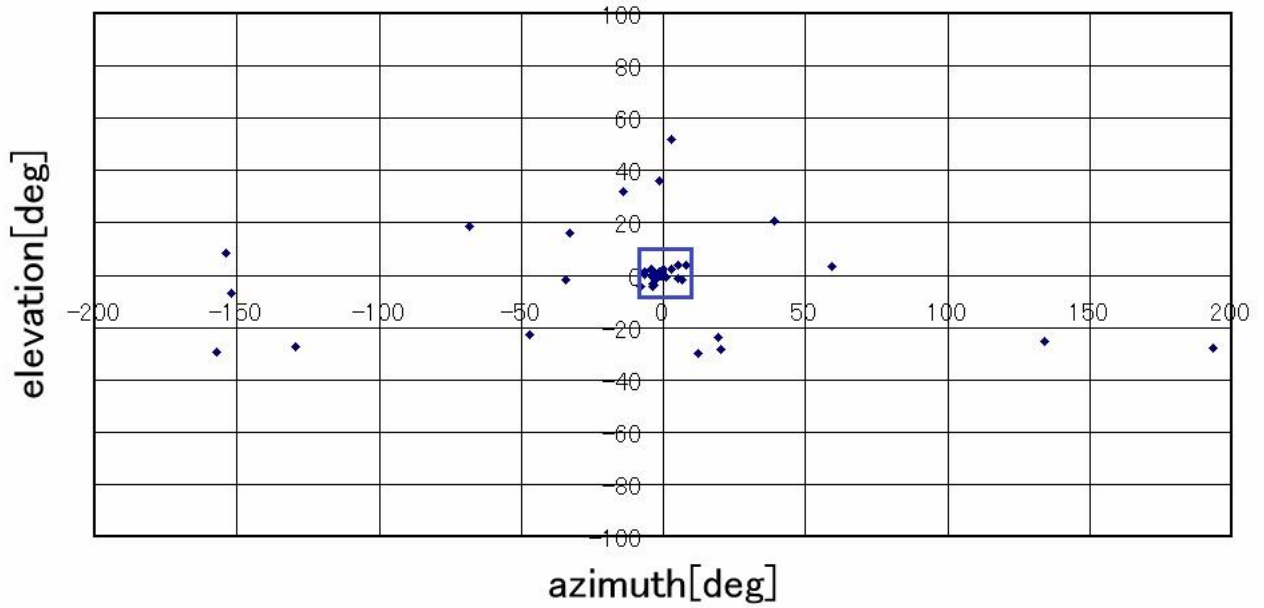


Figure 2.8 Error distribution for azimuth and elevation angles measurements in Tables A.1 and A.2. The square represents 10 degrees error range.

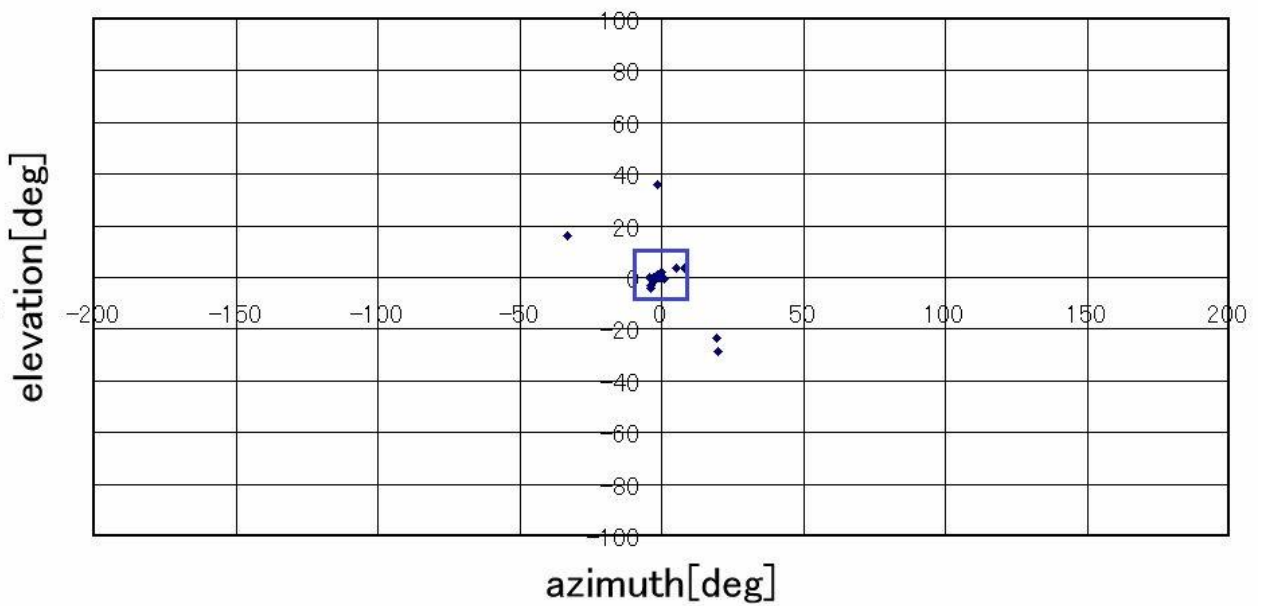


Figure 2.9 Error distribution for azimuth and elevation angles measurements for meteor echoes with duration more than 3 seconds and maximum intensity level (12).

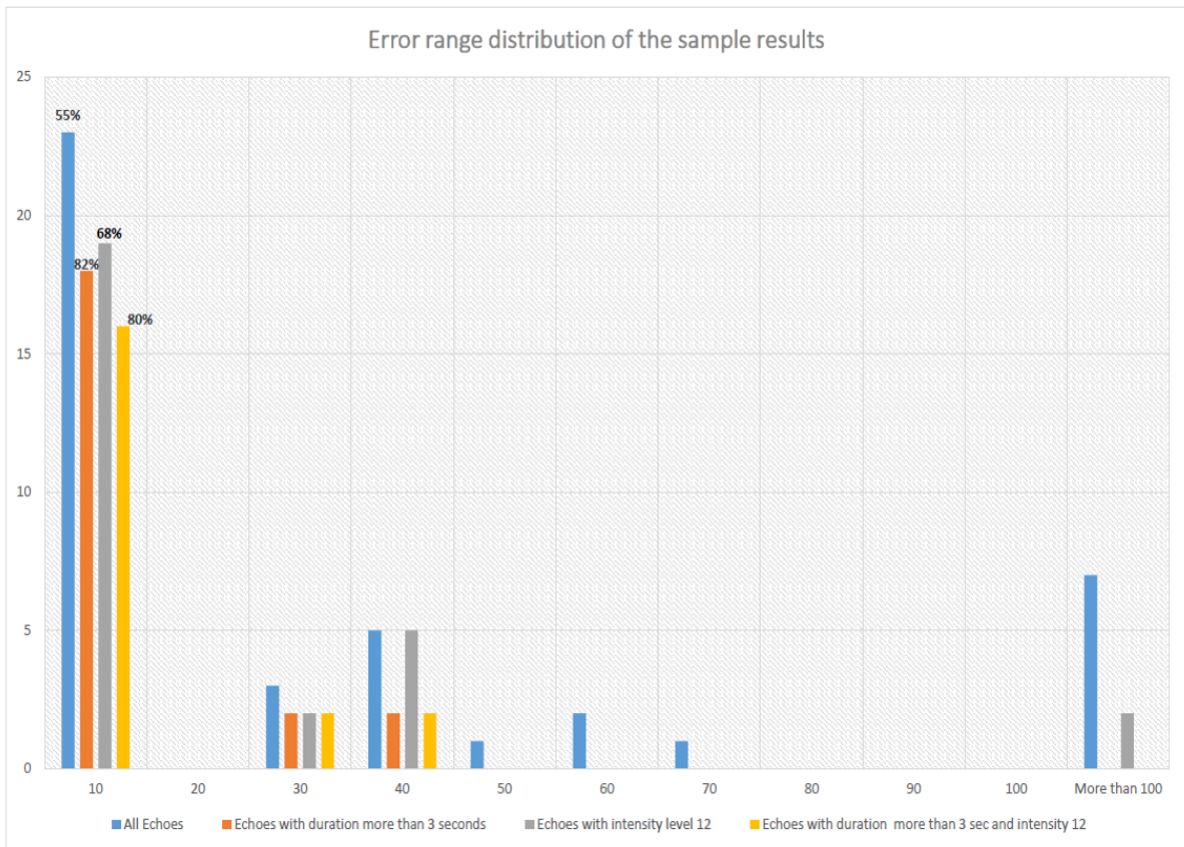


Figure 2.10 Error range distribution for the observational samples in Tables A.1 and A.2. The horizontal axis represents the error range in 10 degree steps for the maximum error among the azimuth or elevation angle measurements. The vertical axis represents the frequency of occurrence within the error ranges. The percentages are for the frequency of occurrence within 10 degrees error for each category.

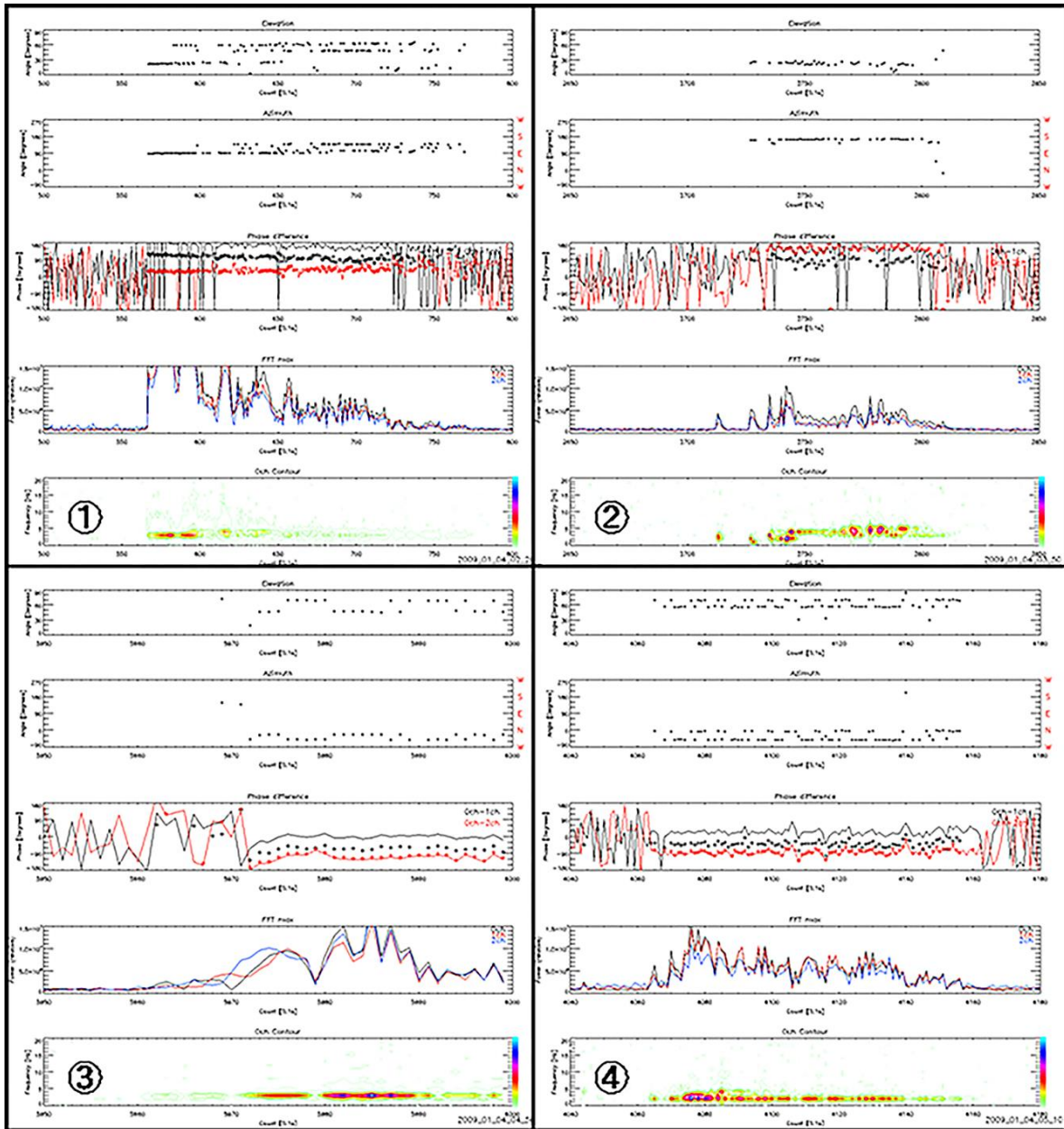


Figure 2.11 The same as in Fig. 2.7 of ‘HRO_IF_VIEW’ graphical output, but for the four mismatched cases with durations more than 3 seconds and maximum intensity level of 12. For the top two panels of azimuth and elevation angles, the plotted data show inconsistent scattered characteristics for cases of (1), (3) and (4). For case (2), azimuth and elevation measurements are consistent but the determined elevation was different from the optical observation.

2.5 Summary

A low cost methodology for meteor echo direction determination using radio forward scattering and the interferometry technique is presented. The developed system uses an image processing algorithm to filter several types of noise echoes and automatically count the number of meteor echoes in real time. It can also analyze the phase difference between 5 channels of received signals and generate text and graphical information about meteor echo directions. A period with simultaneous optical and radio observations was selected to verify the effectiveness of the system methodology and display its capabilities. Although the amount of the selected data remains insufficient to evaluate the constant performance of the system, it gives an indication about the system sensitivity to different types of meteor echoes. The average agreement level of 80% among the selected long duration observation samples (more than 3 s) reflects the system increasing efficiency in observing the direction of meteor echoes of this type. However, the existence of disagreement for some meteor echoes with long durations requires additional statistical analysis over larger amounts of simultaneous radio and optical observational data to verify precisely the effect of surrounding obstacles (buildings and trees) on the interferometer measurements.

The automated measurement of meteor echo directions is considered as the fundamental starting point towards a comprehensive study of meteor origins. Considering the low budget environment, a network of remote single-antenna detectors can gradually be established to provide accurate observation of meteor trajectories and velocities. At the present time, two additional receiving remote stations with single antenna each were established at distances of 23 and 13 kilometres away from the main KUT interferometer location. Future work could focus on developing an accurate automated observation algorithm using the multiple stations that allows the determination of each meteor trajectory and velocity. By observing the trajectory and velocity of each meteor, it might then be possible to not only deduce the orbital parameters of parent comets of meteor streams, but also to statistically study sporadic meteors behavior and deduce other possible origins of meteoroids such as the interstellar meteoroids [22].

CHAPTER 3

Upper atmospheric science

3.1 Introduction

The formation of the meteor ionized trails is subject to several physical and chemical effects that are still under research and investigation by scientists nowadays. Ablation, sputtering, fragmentation and others are examples of the processes describing the ionized trails behavior during its entry to the atmosphere. Basically, the meteoric particles interaction with the atmospheric molecules results in the formation of an ionized column of free electrons striking behind the high speed meteors. The density of the ionized columns varies depending on several factors including the velocity and mass of the meteor. Trails with very low electron density are called “undersense” trails, while those of high electron density are called “overdense” trails. The critical density level that distinguish between both types is in the range of 2.4×10^{14} electrons/m [10]. Underdense trails reflect radio signals randomly from individual electrons resulting in short meteor echoes (~less than 1 second), while the overdense trails act as a uniform cylindrical plasma resulting in longer echoes (Fig. 3.1).

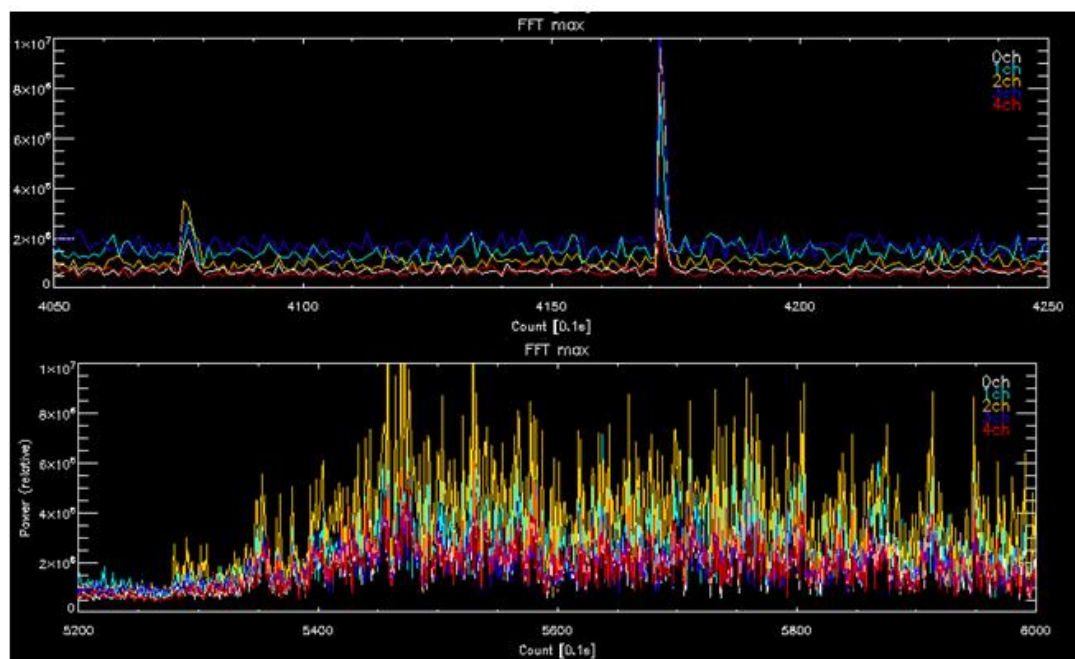


Figure 3.1 Examples of meteor echoes by undersense (up) and overdense (down) trails shown by the HRO-IF-VIEW software.

The ionized meteor trails is considered as an indirect source of information on the mesospheric conditions. The duration of the overdense meteor echoes scattered from the high density meteor trails is directly impacted by the removal rate of the ionized species. Previously, the diffusion of the free electrons was suggested to be the dominant cause behind the removal of the trails and consequently the reduction of the echo durations (e.g. [23]). Subsequent studies speculated the major cause of the removal of the trails to the free electrons attachment to neutral atmospheric molecules (e.g. [24]). Thereafter, the role of the secondary ozone layer in

oxidizing the ionized trails was proposed to be the primary cause of the removal below the 95 km height [25]. The relationship between the ozone deionization process and the overdense meteor echo durations was elaborated by [26]. This relationship was further developed to ozone concentration observation method by [27]. The method uses the knee-shaped curve of the statistical cumulative logarithmic plot of the meteor echo counts versus echo durations during a certain period. The knee point on this curve where the meteor echo counts dramatically drops down is determined as the transition from the diffusion-limited regime to the chemistry-limited regime. As the mesospheric ozone is inversely related to the solar activity (e.g. [28]), the varying position of the knee during the daytime and night time, seasonally or annually can be an indirect observation unit for the mesospheric ozone concentration and the solar activity level.

Having the advantage of longer meteor echo durations, meteor observation by radio forward scattering would normally be a preferred option for this method with respect to the backscattering systems. The basic parameters of meteor echo counts and durations are obtainable by the basic setup receiver configuration of the forward scattering meteor radars, where a single antenna and a single receiver are used. This configuration is spread not only among professionals but also among amateur radio observers worldwide. In Japan there exist more than 100 receiving sites with similar setups. It could be beneficial for this type of observers to add an educational scientific usage to their systems through meteor echo duration analyses. However, the automation of observing and recording the meteor parameters would be required in order to perform a statistical analysis over large amounts of data accurately. The purpose of this chapter is to present a trial to extend the usage of the most basic meteor radar system setup to observe the mesospheric ozone concentration variations. The methodology and the tools used are explained in addition to statistical results during 2 distinct meteor showers; the Perseids and the Geminids. The detailed chemical explanation of the meteor ions reactions with the mesospheric ozone is beyond the scope of this study.

3.2 Methodology

The KUT system constitutes multiple interferometric receivers setup, however, only one receiver was used for the duration distribution analysis and a second receiver was used for duration accuracy check. The interferometric setup was used to estimate height trends as a preliminary step towards a complete vertical ozone concentration measurements.

3.2.1 Duration measurement

The developed software Meteor Echo Counter (MEC) uses image processing algorithm to automate counting of meteor echoes and their durations [21]. The input to the MEC is the HROFFT (Ham-band Radio meteor Observation Fast Fourier Transform) spectrum images generated every 10 minutes. The output of MEC is the same input HROFFT images during the period selected for analysis but with duration measurements marked with superimposed hatches above each overdense meteor echo detected (e.g. Fig. 3.2), in addition to a daily text file summarizing all meteor echo records. The text files are then combined and filtered for the required meteor echo duration conditions. For the KUT forward scattering system, the persistent observation of the signal power profiles showed that the overdense type meteor echoes are usually longer than 1.5 - 2 seconds. Therefore, for the scope of the chemistry-limited analysis, the records were filtered for only echoes with durations more than 2 seconds. The

accuracy of the duration measurements within the KUT system is checked by comparing two receivers' measurements by using the HROFFT in the 2-channels mode.

For the Perseids meteor shower with many long duration echoes the average accuracy was determined to be within $\pm 2 - 3$ seconds range by comparing 2 channels, whereas for the Geminids meteor shower it was within a range of ± 1 second.

As the duration of meteor echoes is dependent on many factors such as the transmitter-receiver distance and the transmitting power level, other systems may have different duration thresholds for overdense meteor echoes. Moreover, other systems may have different duration measurements for the same meteor trails observed. The performed duration distribution analysis is then not targeting to compare with other systems rather than to compare two distinct meteor shower events using the same tools and derive the relative differences.

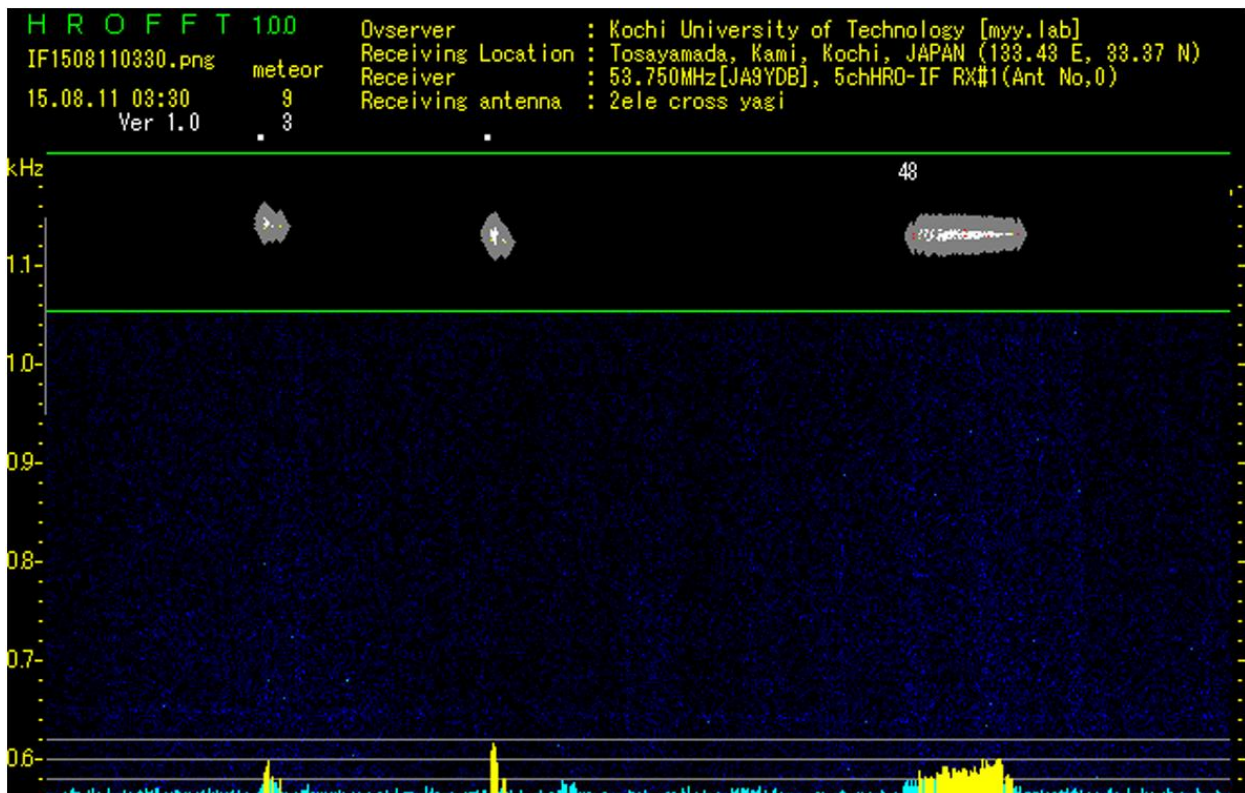
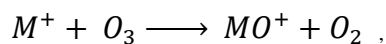


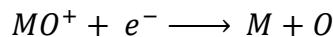
Figure 3.2 Output images of MEC showing the duration above the overdense meteor echoes detected

3.2.2 Ozone concentration observation

With a daily detection average of around 50 overdense meteor echoes during meteor showers for the KUT system, it is possible to plot the cumulative duration distribution against the corresponding overdense meteor echo counts and obtain the knee-shaped curve. The chemical process and radio derivations of this method are detailed in the previous works listed in the introduction and here we simplify the relevant conclusions used in the analysis. The simplified reaction of the secondary ozone layer with the meteor ionized trails occurs in two consecutive steps. Firstly, the meteor ions are oxidized by the ozone:



where M^+ is the meteor ions. The oxidized ions are then combined with the meteor trails free electrons,



The gradual loss of the meteor trail plasma occurs with time constant $T = (\alpha[O_3])^{-1}$.

where α is the oxidization rate of free electrons with ozone ($\approx 2 \times 10^{-16} \text{ m}^3\text{s}^{-1}$).

The ozone concentration at the knee point " T_c " in the duration distribution curve can then be obtained by the relation:

$$[O_3] = (\alpha T_c)^{-1} \dots\dots\dots(5)$$

This relation should generate one ozone concentration value for each duration distribution curve. Therefore, a large number of overdense meteor echoes is required at different height levels to observe the secondary ozone concentration profile vertically. Hence, it becomes necessary to determine the heights of the meteor trails corresponding to the knee position. Despite that it is not possible to determine the meteor height using the basic receiver setup configuration applied here, the relative comparison of the knee position of meteor groups arriving at different times such as day and night or during different meteor showers could be indicative about the mesospheric ozone concentration level.

3.2.3 Height estimation

The geometry of the forward scattering observation systems introduces many complexities to calculate the meteor trail heights. It is not possible to estimate the meteor trail heights from the basic setup configuration only. However, the estimation of the presence of a meteor hot spot near the midpoint path between the transmitter and receiver (*e.g.* [29, 10; 30]) could allow height calculation through multiple receivers interferometric setup for direction finding. In Fig. 3.3, the point 'F' represents the originating signal source from the FNCT station and the point 'K' represents the receiver at KUT. The projection from the reflecting point on the meteor trail 'M' to the ground plane 'P' represents the required height 'h'. The elevation angle ' β ' and the azimuthal angle ' α ' are calculated by interferometric analysis (see Chapter 2). The meteor echoes with ' α ' more than $\pm 90^\circ$ (behind the KUT radar) were not considered in this analysis. The remaining parameter required to calculate the height will then be the receiver range KM or the projected distance along the transmission path 'L'. Neglecting the Earth curvature, it can be possible to estimate the meteor trail heights from the equation:

$$h = L \cdot \tan \beta \sec \alpha \dots\dots\dots(6)$$

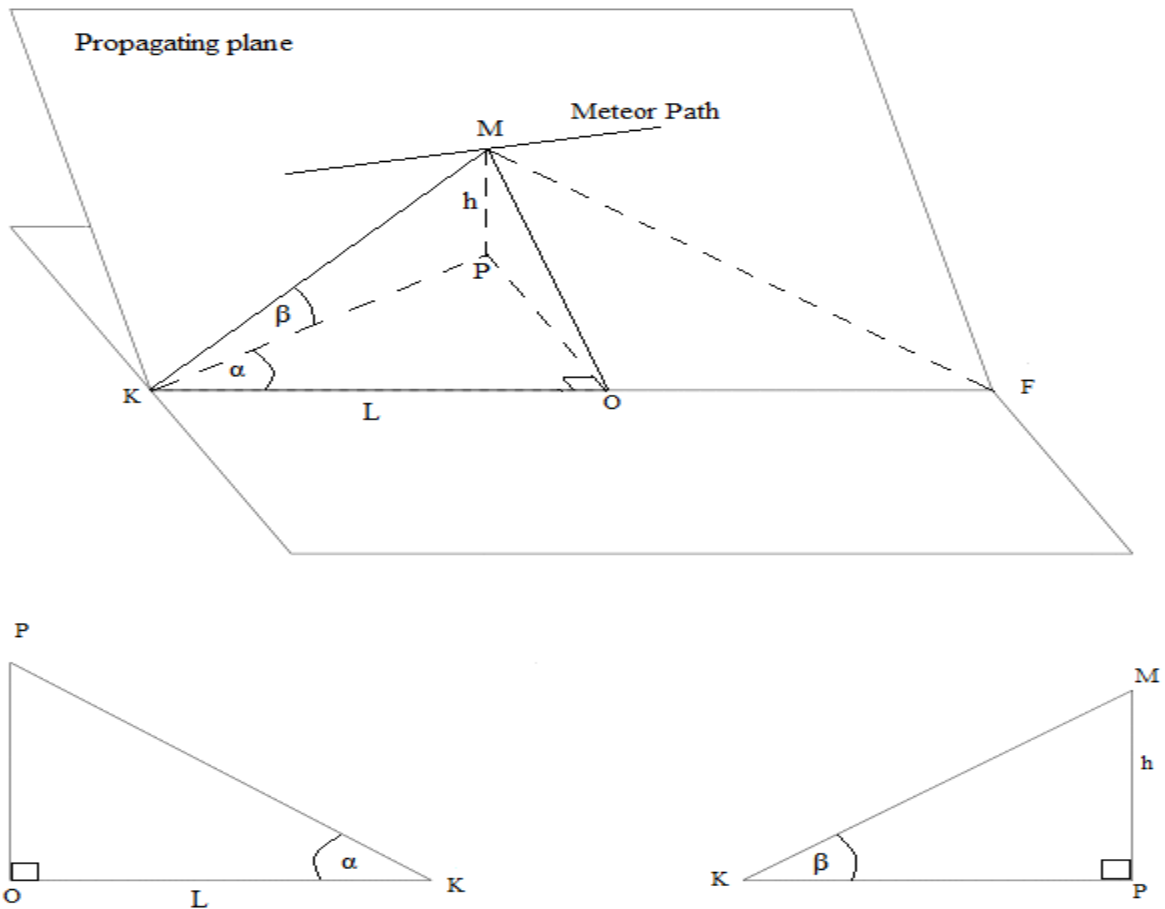


Figure 3.3 Meteor trails height estimation by direction finding.

3.3 Results and Discussion

The two meteor showers Perseids and Geminids were selected for this analysis firstly because the availability of data records in the KUT system since 2005 during the both shower periods can be sufficient for statistical analysis. Secondly, because these two showers represent two streams of distinct characteristics such as occurrence time, velocity and height. For the Perseids meteor shower the selected period for analysis was from August 8th to August 15th, while for the Geminids meteor shower it was from December 10th to 17th. All the overdense meteor echoes during the selected periods were included in the analysis, given that the sporadic overdense meteor echoes normally have very low rates in the KUT system (less than 2% of rates during showers peak time) and can be neglected. Overall, more than 12,000 HROFFT images were analyzed by the MEC software during the selected periods. After filtering the results by duration to only overdense echoes, a total of 2779 overdense meteor echoes for Perseids and 2431 for Geminids were resulted. Although MEC software includes different level settings for noise elimination, meteor echoes longer than the knee durations were manually verified again on the original HROFFT image spectra. This was specifically necessary for the cases of Perseids long duration echoes of more than 40 seconds which is the typical duration range of electromagnetic noise-source interference sometimes seen in the KUT system.

The cumulative duration distributions in logarithmic scale for the Perseids and Geminids is shown in Figs. 3.4 and 3.5, respectively. The Perseids are counted in duration bins of 5 seconds

while the Geminids are counted in duration bins of 2 seconds. The knee position for the Perseids was determined in the duration range of 45 - 50 seconds and for the Geminids in the range of 12 - 13 seconds. The discrepancy in the knee position agrees with the impact of the aforementioned distinct characteristics of the two showers. The velocity and height range of the Geminids was agreed by both optical and radio observations to have lower levels than that of the Perseids (e.g. [31, 26]). Therefore, meteor ionized trails of the Geminids could be more affected by the secondary ozone layer maxima below 95 km. Also, the depletion of the ionized trails of the slower Geminids meteors in the atmosphere is higher than that of the faster Perseids meteors and therefore the loss of the electrons is higher, thus moving the knee position of the Geminids to an earlier stage.

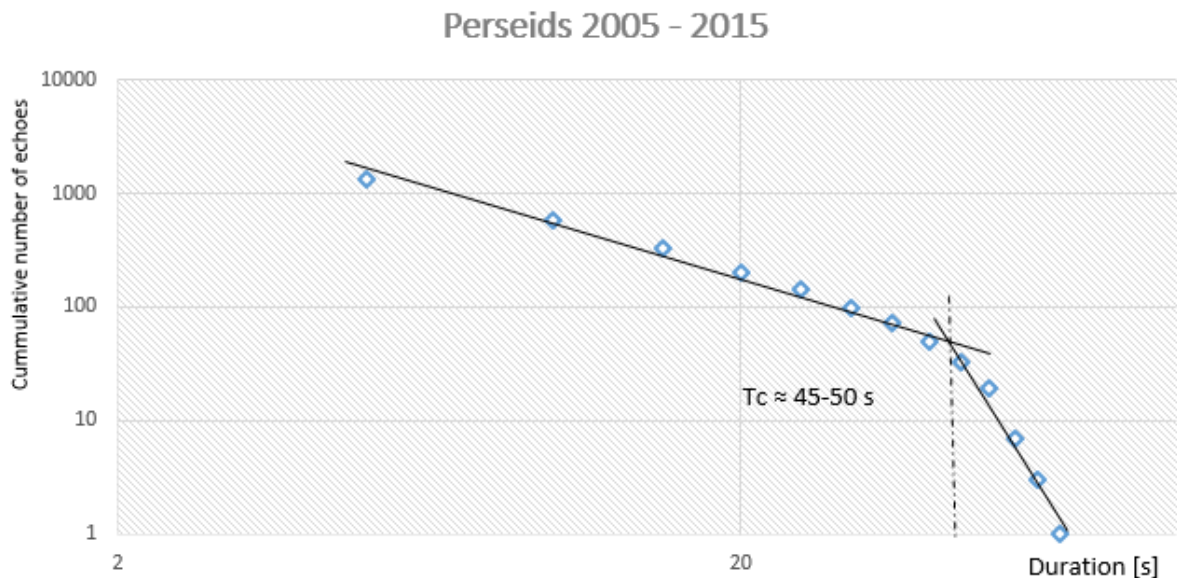


Figure 3.4 The duration distribution of the Perseids overdense meteor echoes from 2005 to 2015.

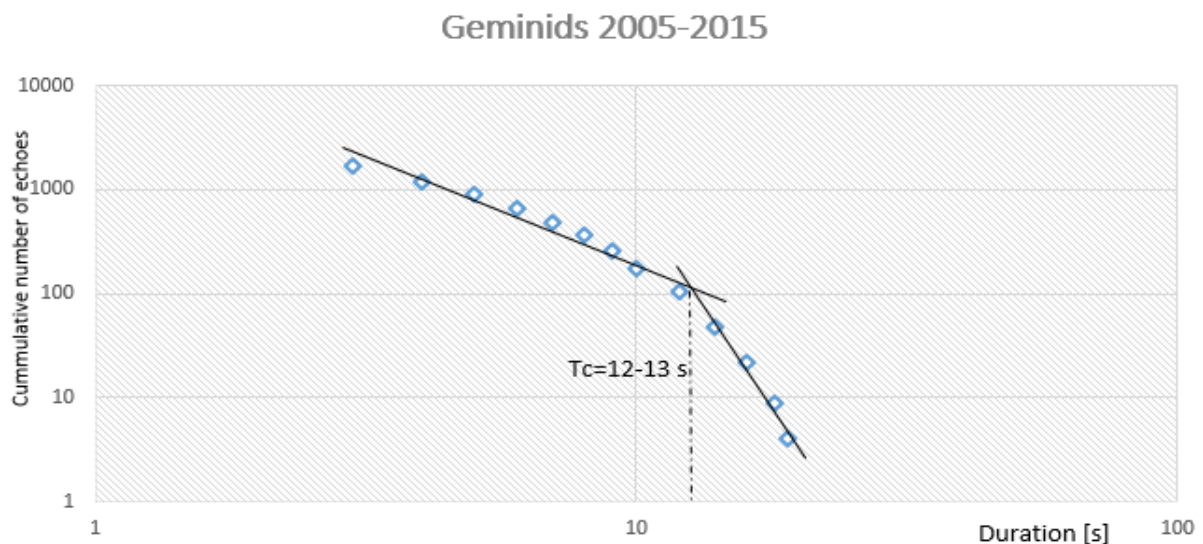


Figure 3.5 The duration distribution of the Geminids overdense meteor echoes from 2005 to 2015.

In order to estimate the heights of the meteor trails corresponding to the knee, we attempted to use the method in Subsection 3.2.3 to analyze the elevation and azimuth angles of a sample of meteor echoes at the knee during the peak period of the two showers. The height trend as a function of the unknown transmission path distance ‘L’ from KUT is shown in Fig. 3.6. This height trend is although logic from the perspective of lower height levels of Geminids than that of the Perseids, it contradicts the existence of a hot spot in the forward scattering systems around the midpoint of the transmission path. Following this trend, at the midpoint distance of 170 km, the Perseids heights would measure ~200 km and the Geminids ~170 km. This is impractical not only because it is uncommon height for meteors but also due to the echo ceiling effect for the frequency used of 53.75 MHz [12]. The uncertain height trend has been included in this analysis to point out the possibility of reaching a vertical ozone concentration measurement method by estimating the meteor positions. The positioning is achievable in the basic radar setups by the addition of two remote receiving stations.

To illustrate an example showing the calculation method of the vertical ozone concentration, a range for the distance ‘L’ from 75 km to 80 km was assumed (Fig. 3.6). By using Eq. (1) for an average ‘ T_c ’ of 47.5 s for the Perseids and 12.5 s for the Geminids to calculate the ozone concentration, the results in Fig. 3.7 were obtained. The obtained values although do not coincide with the satellite measured values but the difference between the Geminids and the Perseids agrees with the decreasing trend. This preliminary figure is only for the sake of showing a practical example and the complete figure could be reached with more meteor showers data associated with the specific heights of each.

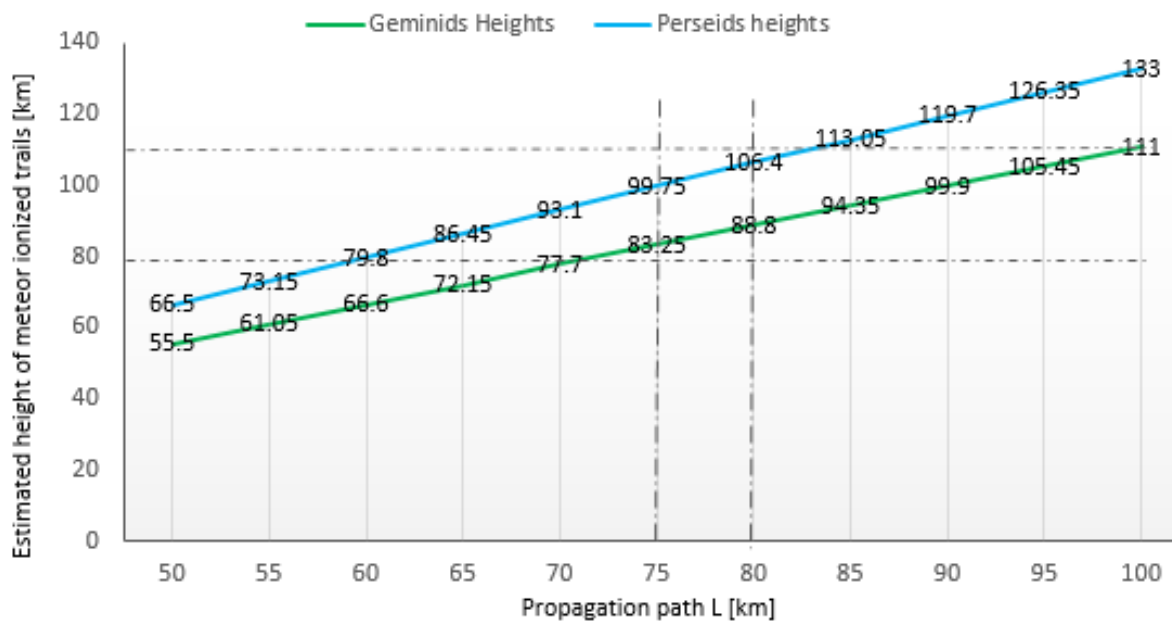


Figure 3.6 Heights of Perseids and Geminids meteor echo samples at the knee in vertical axis versus the propagation path distance ‘L’ in the horizontal axis. The horizontal dashed lines represent the average meteor height region (80–110 km). The vertical dashed lines represent the used range in the height estimation example.

The observation of the mesospheric ozone concentration variations could allow indirect observation of the 11-years solar cycle activity. The annual data records however were not

complete for all years and for some years were totally missing. To observe the 11-years solar cycle activity, two years were selected that has full uninterrupted data records with 5 or 6 years separation. The knee positions of the Geminids 2006 and Geminids 2011 representing low and high sunspot number progression levels (Fig. 3.8) are compared in Fig. 3.9. The knee position for Geminids 2006 is observed at duration range of 8 - 9 seconds which is less than the average Geminids knee durations. This although agrees with the impact of lower solar activity and the increase in the ozone concentration level in 2006, there can be other factors impacting the radio detection rates for the 2 single years such as the varying flux nature of the Geminids shower itself [32]. The continuous annual analysis of the Geminids duration distribution for the whole 11-years solar cycle becomes essential to confirm the solar cycle activity observation by this method.

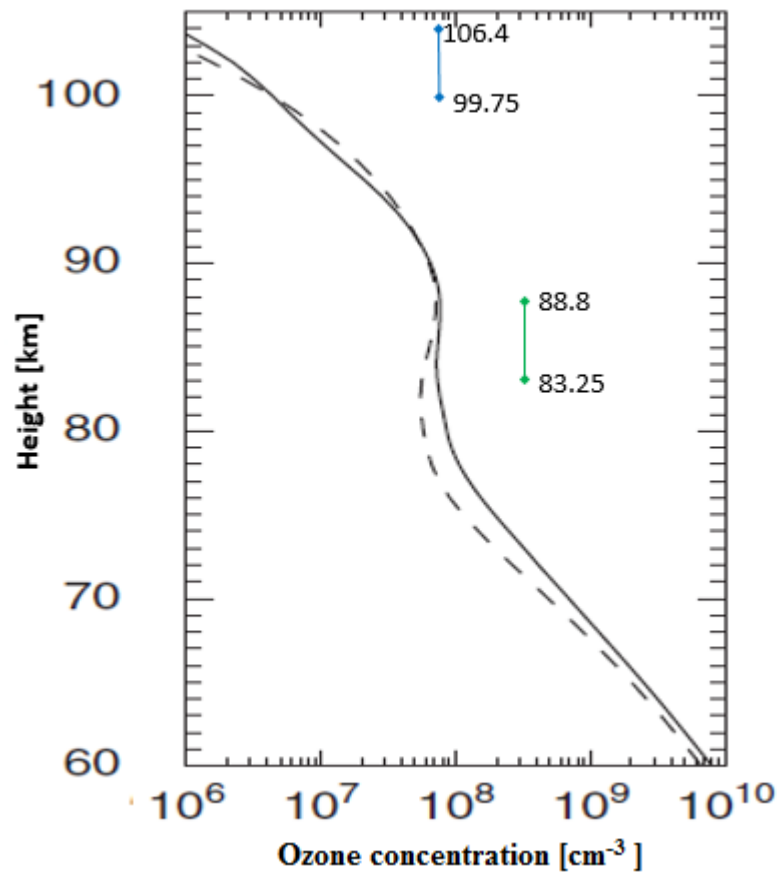


Figure 3.7 Vertical ozone concentration profile (in cm^{-3}) calculated using the knee curves of Perseids (in blue) and Geminids (in green) by (5) and (6) compared to the SABER satellite measurements averaged over all seasons from January 2002–July 2012 (after [33]). The height ranges corresponds to the selected range of ‘L’ from 75 km to 80 km.

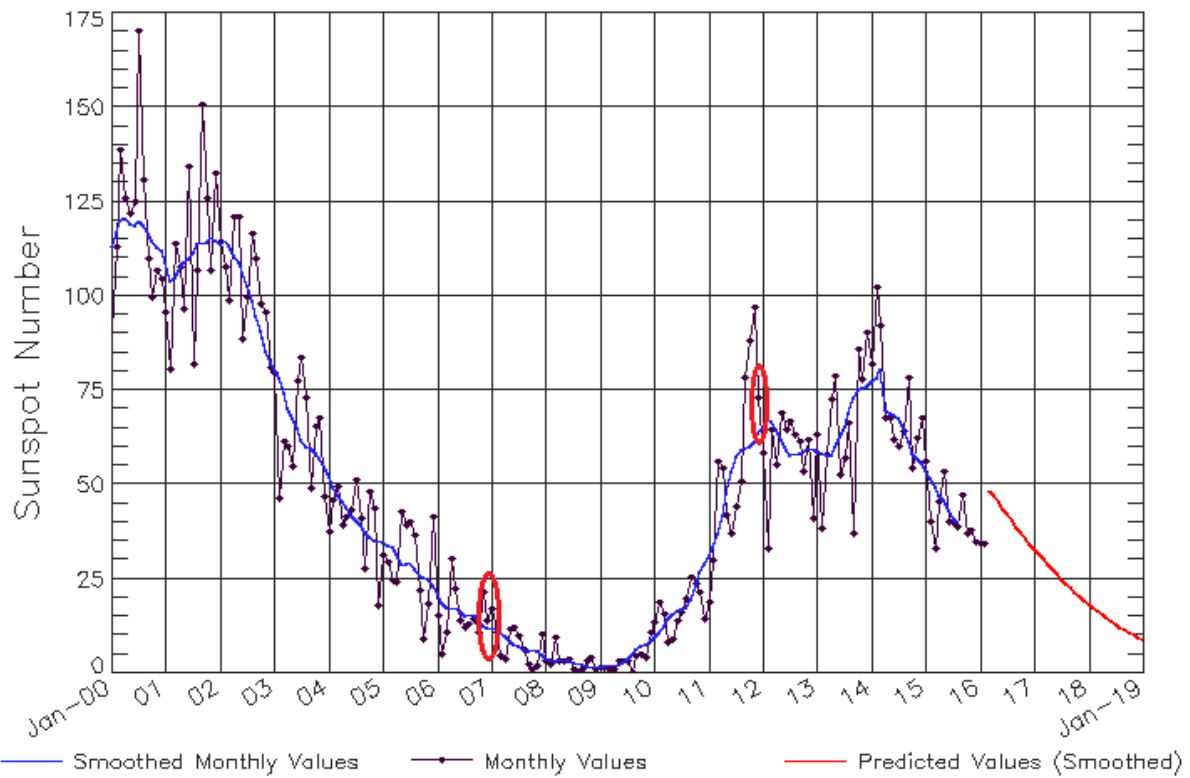


Figure 3.8 Solar sunspot progression of the current solar cycle activity since 2000 (NOAA/SWPC). Marks with red show the points of comparison.

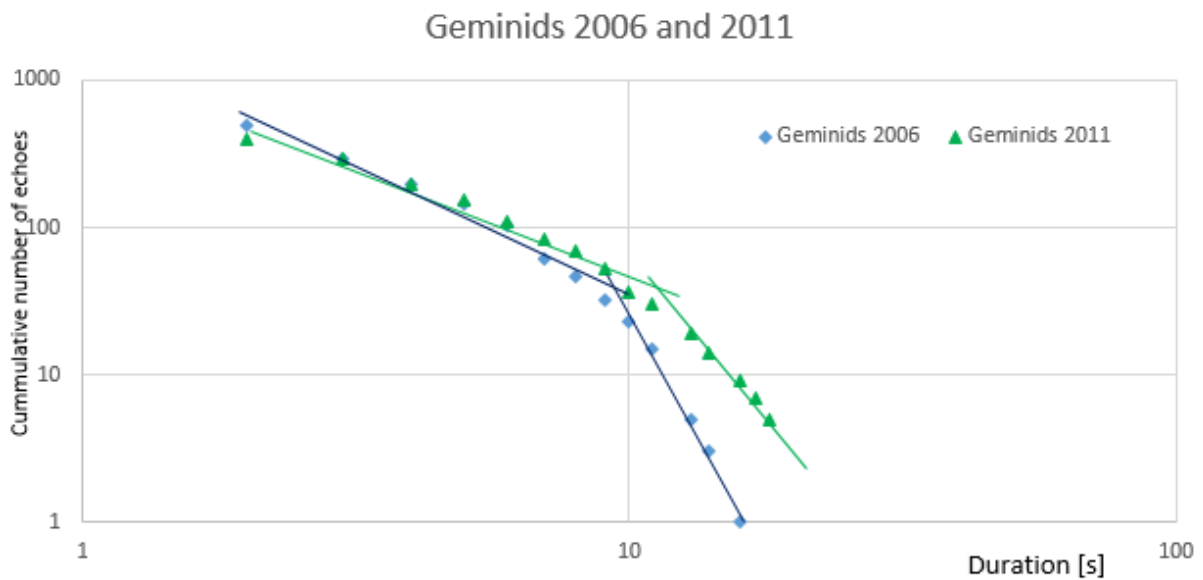


Figure 3.9 The duration distributions of the Geminids 2006 (minimum solar activity) and Geminids 2011 (maximum solar activity).

3.4 Summary

A trial to use a low cost meteor radar basic setup in observing the mesospheric ozone concentration and the solar cycle activity was performed. Although exploratory, this method provides some insight into the role of the secondary ozone layer in the removal of the meteor ionized trails. The obtained knee positions are generally in agreement with the expected mesospheric ozone conditions in the selected cases. Up to this system setup level, the knee duration can be the observation unit for ozone concentration variations. The method can be enhanced further to measure the vertical ozone concentration profile by introducing two remote receivers to determine the meteor trail positions and hence estimate meteor heights. Also, the comparison of 2 single years at the solar cycle halfway can be considered as a partial solar activity observation and it can be ideally confirmed by tracking the annual duration distribution for a whole 11-year solar cycle.

The used method should be applicable in observing the relative duration differences within the same meteor radar system. To standardize the method and compare results of different systems, it might be mandatory to reach a common agreement on the minimum number of overdense meteor echoes required to recognize the knee curve. It is also important to consider the impact of using different frequency, power, transmitter-receiver distance and method of duration measurement on the resulted durations. Similar meteor radar setups as well as amateur observers are encouraged to perform similar analysis and share the duration distribution curves resulted from different meteor shower events on different places on Earth. Observers using the HROFFT software could benefit from the developed MEC software that was made free for use in worldwide.

CHAPTER 4

Meteor Burst Communications (MBC)

4.1 Introduction

The determination of the role of the meteor ionized trails in the forward scattering of radio signals during the early 20th century has gradually raised the interest in developing Meteor Burst Communication (MBC) systems. Several MBC systems were developed since then relying on the entry of millions of meteoric particles daily to the Earth's atmosphere as a natural communication medium such as the JANET system in Canada [34], the military COMET system in Europe [35], and the SNOTEL system in Alaska, USA which is still operating till now [36]. In Antarctica, several attempts for establishing MBC systems for data collection from remote sensors were performed (*e.g.* [37]). The use of MBC on Mars was also proposed as a lower cost option for communication on Mars [38]. Currently, a few MBC companies in the USA and Europe are still providing commercial telemetry and tracking services. Despite the various advantages of MBC of cheaper equipment costs, almost free running costs and availability at any location, the randomness nature of the MBC link and the weak mobility options have failed to let MBC practically compete with other emerging technologies such as the satellites or cellular networks during the last two decades.

4.2 Motivation

The MBC system is generally a complex system involving several scientific and engineering design considerations. Within the educational scope of the KUT meteor research group, MBC research was recently launched as a rich hands-on experience for graduate students on providing engineering solutions. In addition to that and likewise the existing gap in the instrumentation used in the astronomy and atmospheric science meteor-related studies, there exist a wide gap in certain locations on Earth where either the expensive satellite links are the only available or no communication is possible at all. Similar to the situation in Alaska, several remote locations worldwide endure the same conditions; vast areas, very low population and extreme weather conditions. Such conditions do not make it a very attractive option for cellular or fixed-lines telecom operators to invest in. An example is the situation in the Saharan desert in North Africa or in the Antarctica where satellites become the only available tool for long distance communications. Although the satellite links are convenient in these areas, it becomes an expensive option on the long run and risky as the sole method of communication. Additionally, the rapid developments in the last decade in the Machine to Machine (M2M) and Internet of Things (IoT) applications have introduced several scenarios in transportation, telemetry, remote assets monitoring and other applications that require transferring data from remote areas at low data rates. The value engineering might then be considered in evaluating the possibility of using MBC as an alternative or a backup low cost option to the satellites for these low speed data applications.

The usage of the ham-band radio for MBC can provide several advantages due to its growing spread worldwide, easy licensing and availability of various equipment providers. Also, the ham-radio user communities could have a positive role in the case when they listen to the random MBC signals that are not delivered to the desired destination and voluntarily forward them. Whereas there currently exist several techniques with proven performance in the meteor

scatter amateur work such as the computer program WSJT (Weak Signal communications, by K1JT), the connectivity options of the ham-band networks could be a unique feature that can add more flexibility and simplicity to the MBC systems. The wide spread of the ham-band radio network repeaters can provide extra connectivity options as they could be reachable from distant rural areas through MBC. Moreover, as most of the activities in remote areas are not performed in fixed locations, it is required to minimize the size of the system to allow mobility from place to place. Recently, several ham-band radio transceivers were developed to provide a stable interface to Android devices which would minimize the MBC stations size. Lastly, the low cost amateur setups could be reasonable for small industries and common people who cannot afford the long term running costs of the satellite link. On the other hand, the wireless characteristics of the MBC channel constitutes several design considerations that need to suit the wireless characteristics of the ham-band radio networks. The purpose of this chapter is to present a preliminary study on the potential use of D-STAR (Digital Smart Technologies for Amateur-Radio) network for MBC. The scope is focused on the wireless part only as a first step before complete end-to-end solutions is considered. An experimental setup by initial low power transmitters described although was not successful to prove the concept, the setup information might provide an adequate startup background for interested amateurs or experts to try a more advanced level of experimental setup. Expertise in MBC, antenna design, ham-band radio and Android software development could add a deeper insight on the topic.

4.3 D-STAR for MBC

D-STAR is a protocol developed by the Japanese Amateur-Radio League (JARL) in 2003. The protocol is open to manufacturers to develop any equipment that complies with the standards. In the last decade, the number of D-STAR users and repeaters have shown enormous growth worldwide and are still rapidly growing till now. This rapid growth was the main motivation for us to evaluate the possibility of utilizing it in favor of MBC. The recent D-STAR enhancements by ICOM Company providing a stable interface to Android devices was another reason so as to minimize the size of the overall system and provide a compatible interface to a wide range of sensor applications. The basic operation of D-STAR is presented before a preliminary evaluation of D-STAR as a protocol for MBC is explained in the upcoming subsections.

4.3.1 D-STAR operation

D-STAR provides simultaneous digitized voice and data communication through two modes: The digital voice mode (DV) and the digital data mode (DD). In the DV mode, voice and data streams are transferred at a rate of 4800 bps. The stream is divided into digitized voice at a rate of 3600 bps using the AMBE (Advanced Multiple Band Encoding) 2020 codec and 1200 bps for low speed data. The DV transmission works on 3 different frequency bands: 144MHz (C band), 440 MHz (B band) and 1.2 GHz (A band). In the DD mode, high speed data can be transmitted at 128 kbps. The DD mode is dedicated to data only without voice and works only on the 1.2 GHz band.

D-STAR has a network hierarchy where users have several options for communication. The basic option is the simplex direct communication between two users where line of sight (LOS) exists. In this type users configure the radio transceiver call sign fields of MY (User's own call sign) and UR (Destination user's call sign). In case of longer distances or the presence of obstacles between users, it is possible to use a local repeater within the same D-STAR zone. An additional call sign of the repeater (RPT1) will have to be configured. If the users are located

at any location in the world where a D-STAR repeater exist with a gateway capability, communication can be made through internet by registering both the transmitter and receiver to a local gateway repeater. The details of the several routing options of the D-STAR network can be found in any ICOM D-STAR transceiver manual. The basic differences are summarized in Fig. 4.1.

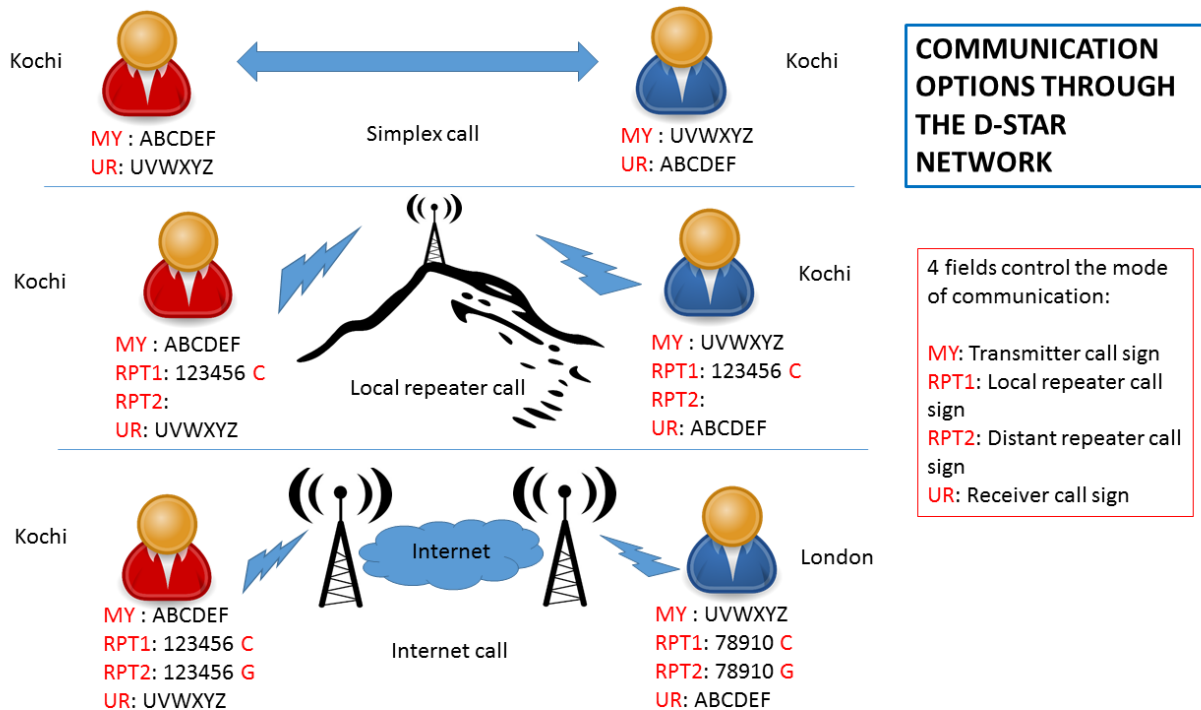


Figure 4.1. Communication options through the D-STAR network.

4.3.2 MBC connectivity

The connectivity options of D-STAR remain valid for MBC long distance communications. In case of using a gateway repeater for reception, the MBC system can take advantage by eliminating the need for constructing a receiving station. This is only applicable in case the whole transmitted data burst is delivered correctly as the call signs are needed for the routing to the final destination. Additional receiving stations can be constructed in different locations in parallel for simplex mode operation so as to increase the probability of reception.

In order to clarify the connectivity options that are beneficial for MBC applications, we take a closer look at the situation in the Saharan desert in North Africa. The Saharan desert is the largest hot desert in the world with an approximate area of 9,200,000 square kilometers. The coverage of the cellular networks in the Saharan desert area shown in Fig. 4.2 constitutes less than 15% of the land. Away from these areas, long distance communication is available only through satellites. Ham-band radio exists for short distances with absence of repeaters. Despite the low population, several activities take place in the deep desert areas regularly. Industrial products are transported for long distances, industrial mining of gas and petroleum, archaeological exploration missions and many others. Among these activities, several low speed data communication applications exist. Also, for common people exploring the desert in scientific missions or travelling in long off-roading Safari trips, a backup emergency communication tool can be a necessary requirement. As mentioned earlier, it is risky to rely

solely on satellites in these applications and therefore the MBC can be an efficient candidate to fill this gap.

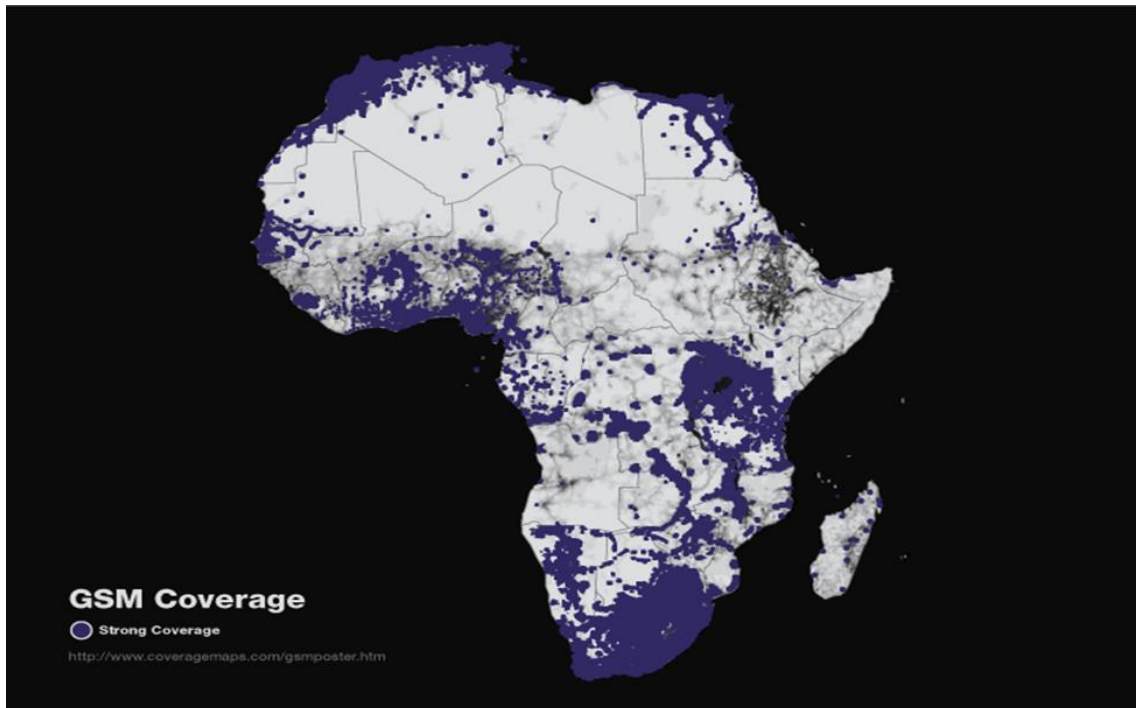


Figure 4.2 Cellular networks coverage in the Saharan desert (Credit: coveragemaps.com).

Consider an M2M scenario where temperature-sensitive products are required to be transported between two distant cities across the Saharan desert in Egypt. It is required to report the temperature of the product containers in regular intervals of less than 30 minutes to the company base in Cairo. Zooming-in more on the cellular coverage map in Egypt (Fig. 4.3), it is normally concentrated around the populated Nile Valley and the northern and eastern coasts. There will be two options for using MBC that can be applied simultaneously. The first is to construct a full master station to receive the meteor bursts transmitted from the moving trucks. In this option, the connectivity is simplex and the company has full control on the communication protocol. The second option is to use a D-STAR gateway repeater, where the transmitter must register the D-STAR transceiver to the nearest repeater beforehand. The current D-STAR repeater list worldwide is updated regularly through the website (<http://www.dstarinfo.com>). Until this paper was written, no D-STAR repeaters appear to be installed in the Saharan desert. However, there exist several repeaters in the southern Europe that can be reachable through the long distance MBC links from the northern areas of the desert (Fig. 4.4). In Fig. 4.5, the closest C-band repeater in Cyprus (5B4CY) can theoretically be reachable from the whole desert land in Egypt by MBC. After registering the transmitter and the receiver to the repeater, the 4 fields in the D-STAR transmitter should be configured as follows:

MY: The call sign of the transmitter, for example: ABCDEF.

RPT1: The call sign of the registered Cyprus gateway repeater followed by the frequency band letter, in this case 5B4CY C.

RPT2: The call sign of the local gateway repeater of the receiver followed by the letter G indicating gateway connection, in this case 5B4CY G.

UR: The call sign of the receiver in the company, for example: UVWXYZ.



Figure 4.3 Cellular coverage in Egypt (Credit: Etisalat Egypt).



Figure 4.4 D-STAR repeaters in southern Europe (Credit:dstarinfo.com).

On the receiver side, if no master station exists, it could be enough to connect a D-STAR DV Dongle to a PC and register the call sign to any D-STAR gateway repeater through the website: http://www.dstargateway.org/D-Star_Registration.html. In this case only one way “blind” broadcast communication will be possible from the transmitter to the repeater. If the company has its own receiving station constructed, the increased probability of receiving the transmitted bursts through any of the two paths would improve the performance. It is essential to note that the registration to a specific repeater is a must. Therefore, to cover the whole Saharan desert the nearest repeaters in southern Europe can be used for now. Repeaters in Greece, Malta, Italy and others can cover large areas in the Saharan desert northern part in Tunisia, Algeria and Morocco. The southern part of the Saharan desert will require installing repeaters in North or Middle Africa at locations that can be optimally designed in a separate study.

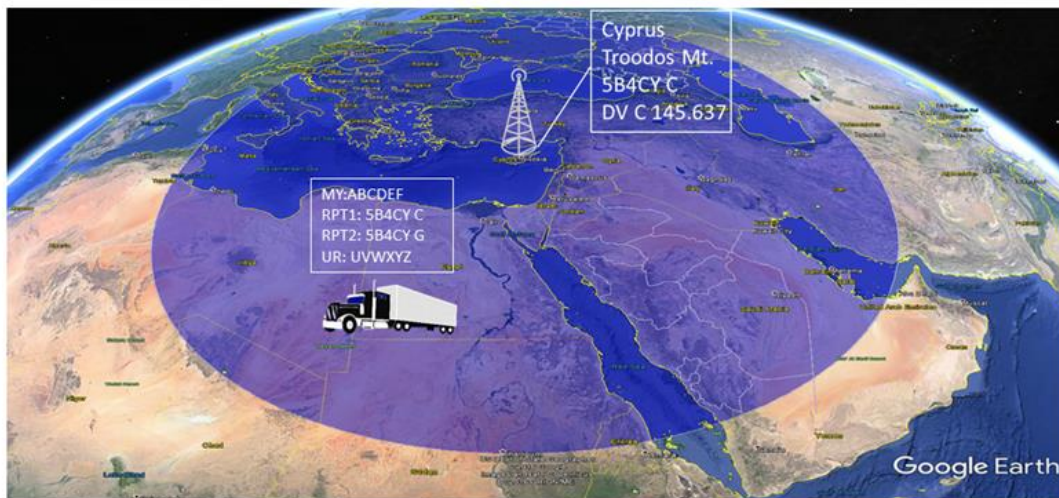


Figure 4.5 The nearest D-STAR C-band gateway repeater in Cyprus with theoretical MBC coverage area of ~2200 km.

4.3.3 Frequency

The meteor ionized trails with very low electron density are called “undersense” trails, while those of high electron density are called “overdense” trails. The critical line density level that distinguish between both types is around 2×10^{14} electrons/m [39]. Underdense trails reflect radio signals randomly from the individual electrons resulting in short meteor echoes (~less than 1 s), while the overdense trails act as a uniform cylindrical plasma resulting in longer duration echoes. The underdense type is more frequently occurring and based on which most professional MBC systems rely on. Although the overdense type trails occur less frequently, scattered signals by overdense trails are of better quality due to the longer trail decay time. The power amplitude of the forward scattered signals by the underdense meteor trails is described by [10]:

$$P_R = \frac{P_T G_T G_R \lambda^3 \sigma_e}{64\pi^3} \frac{q^2 \sin^2 \gamma}{(R_T R_R)(R_T + R_R)(1 - \sin^2 \phi \cos^2 \beta)} \dots \dots \dots (7)$$

where,

P_R Received power.

- P_T Transmitter power.
- G_T Transmitting antenna gain.
- G_R Receiving antenna gain.
- λ Wavelength.
- σ_e Scattering cross section of a free electron.
- q Meteor trail electron line density.
- γ Angle between the electric vector of incident wave and the line of sight to the receiver.
- R_T Distance from the transmitter to the trail.
- R_R Distance from the receiver to the trail.
- ϕ Angle of incidence/reflection.
- β Angle between the trail and the plane of propagation.

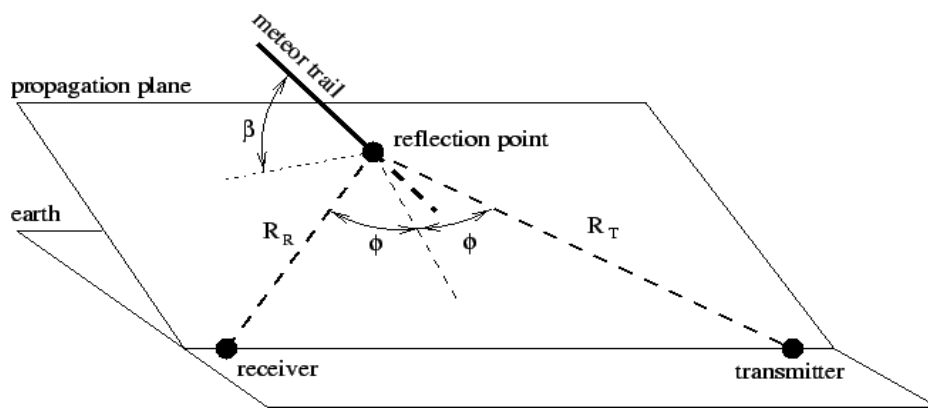


Figure 4.6 Geometry of radio signals forward scattering by meteor trails.

The incorporated noise impacting the reception of the meteor scattered burst including galactic noise and the receiver thermal noise is expressed by [40]:

$$N_o = kT_o \left[\frac{104}{L_R} \left(\frac{\lambda}{15} \right)^{2.3} + F \right] \dots\dots\dots(8)$$

where,

- k Boltzmann's constant = 1.38×10^{-23} J/K.
- T_o Room Temperature = 290 K.
- L_R Power loss between the antenna and the receiver.
- F Receiver noise figure.

From (7), the power amplitude of the received signal is proportional to λ^3 . *i.e.*, the higher the used frequency, the weaker the forward scattered signal amplitude (Fig. 4.7). The case of overdense meteor trails is more difficult to model, however the relation of the scattered signal amplitude to the frequency used remains inversely proportional. As a result, the recommended operating frequency for MBC is generally in the 40-70 MHz range. Lower frequencies are not normally used to avoid the ionospheric disturbances, while the higher frequencies result in fewer correct bursts received. On the other hand from (8), the higher frequencies are less immune to noise effects at the receiving site.

The DV mode frequency band “C” in the 144 MHz range is the lowest frequency available in the D-STAR system that can be used for meteor scatter operation. Although this frequency is not used in the professional meteor observation or communication systems, it is commonly used among the radio amateur groups. To compensate for the degradation of performance expected at this frequency, transmitted power should be at higher levels while using higher gain antennas. A design tradeoff appear here between increasing power and minimizing cost, and also between using high gain antennas of narrow beams on the expense of illuminating wider areas in the sky. The confirmed benefit of using higher frequency is the advantage of decreased antenna sizes that can be more practical for mobile applications.

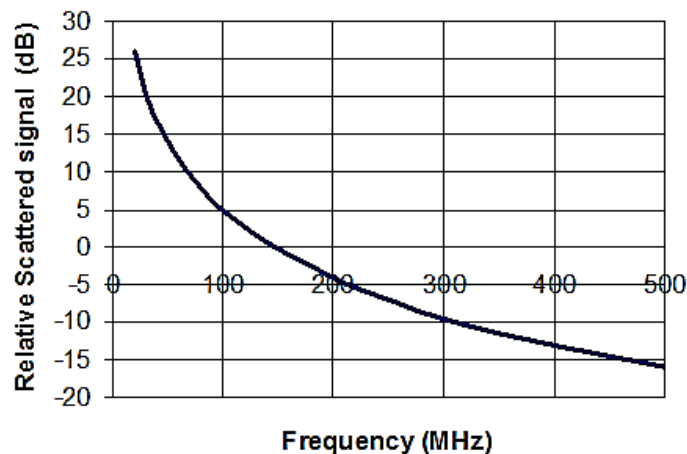


Figure 4.7 Scattered signal relative amplitude in relation to the used frequency.

4.3.4 Burst size

In the DV mode, voice is digitized and sent along with data in a stream of frames (Fig. 4.8). Although voice does not exist in the DV low speed serial communication mode, the allocated bits for voice are filled with spaces and the size of the burst transmitted depends on the amount of data transmitted. The burst size or burst duration is one of the main parameters impacting the MBC systems performance. A direct proportional relation exists between the burst size and the signal-to-noise ratio (SNR) required [41], *i.e.* as the burst size increases, the SNR required increases. The essential information required then was the size of the minimum transmitted burst that can be enough for a single sensor reading of 2 or 3 characters or for an emergency SOS message. The specific frame structure in case of low speed transmission is not clearly defined in the D-STAR documentation so we had to test several message sizes in-lab using the ICOM Android RS-MS1A application connected to a D-STAR transceiver. In Fig. 4.9, the time domain signal detected on the oscilloscope for an SOS message transmitted by the low speed DV mode is shown. The duration of the burst is in the range of 750 ms, which is considered relatively large for scattering by short underdense trails. The decay time of underdense meteor

trails is estimated by the equation:

$$T = \frac{\lambda^2 \sec^2 \phi}{16\pi^2 D} \dots\dots\dots (9)$$

where,

ϕ half the reflection angle (Fig. 4.6).

D Meteor trail diffusion coefficient

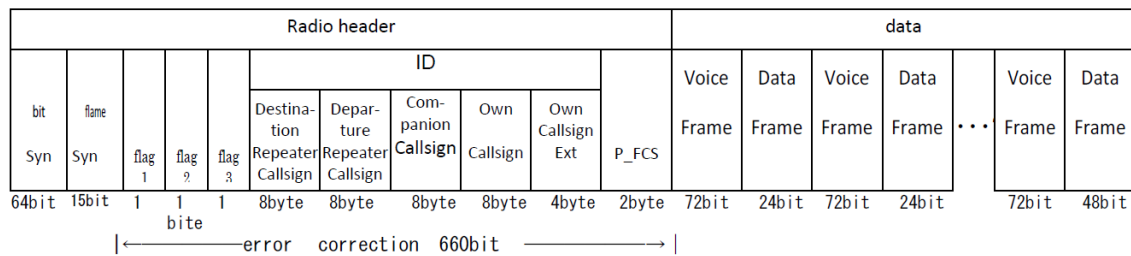


Figure 4.8 The DV frame structure.

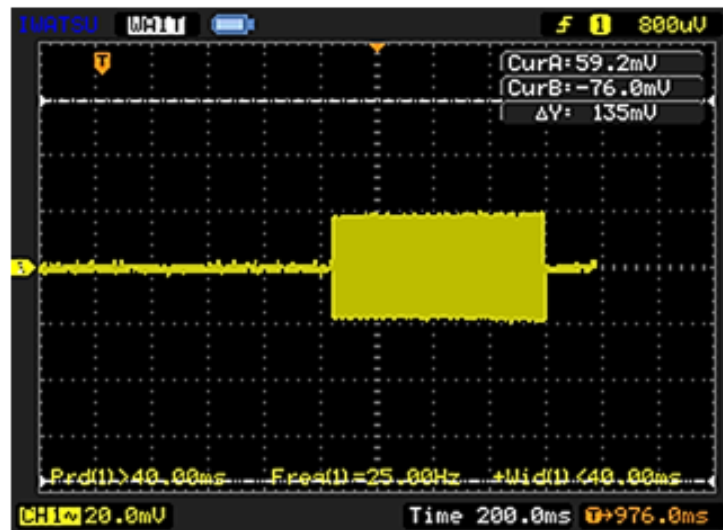


Figure 4.9 Time domain signal of an SOS message transmitted by the Android RS-MS1A application in the DV mode.

From (9), the used high frequency once again shows a negative impact on the scattering duration (Fig. 4.10). It is also shown that as the reflection angle “ ϕ ” increases the decay time “T” increases, thus allowing longer scattering duration. Consequently, as the distance between the transmitter and receiver increases the performance is improved by increasing the probability of exceeding the transmitted bursts size. The maximum distance is however limited by the power used for transmission. As a general result, the successful delivery of the low speed DV burst size would have a better scattering chance by long duration overdense trails over long distances.

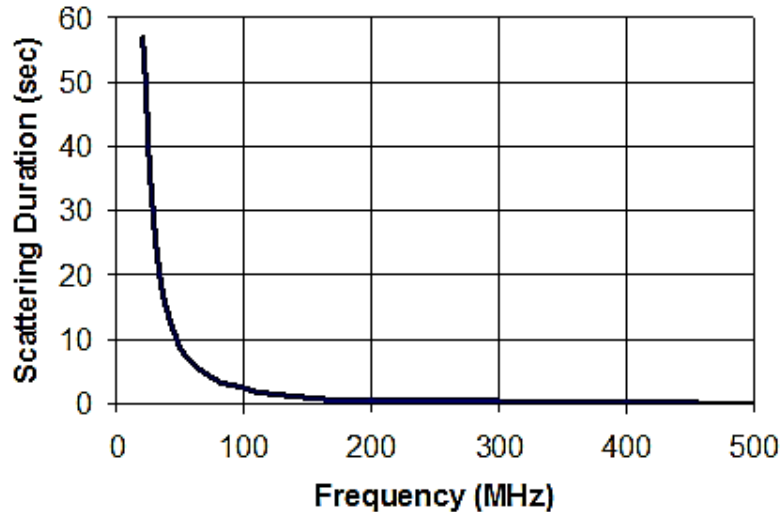


Figure 4.10 The meteor scattering duration by underdense trails in relation to the frequency used.

4.3.5 Capacity

The low efficiency of the amount of useful data in a single transmitted burst might limit the capacity of the system in order to maintain a minimum burst size. As more characters are added to the transmitted burst the size of the burst gets longer and the probability of bit error increases. This in turn would prevent transmitting the readings of multiple sensors simultaneously. The latest enhancements for some D-STAR transceivers featuring Bluetooth connectivity to Android devices can provide a work around to extend the capacity of the system. An example is the D-STAR ICOM ID5100 transceiver that allows up to 8 Android devices to be simultaneously connected via Bluetooth to the transceiver. While the transceiver manual states that not all the 8 devices can be of the same type (headsets or data devices), it is not mentioned whether there is a certain maximum for one type [42]. Assuming there can be 2 to 7 Android devices paired simultaneously to the same receiver, each of these devices can be paired to several Bluetooth-interfaced sensors such as the Arduino board sensors. Using Android software applications, sensors can be programmed to send their readings in minimum bursts subsequently in a manner similar to the time division multiple access (TDMA). However, the more sensors sharing the same transmitter, the less the number of transmission trials for each and consequently the less probability of finding a usable meteor trail for each.

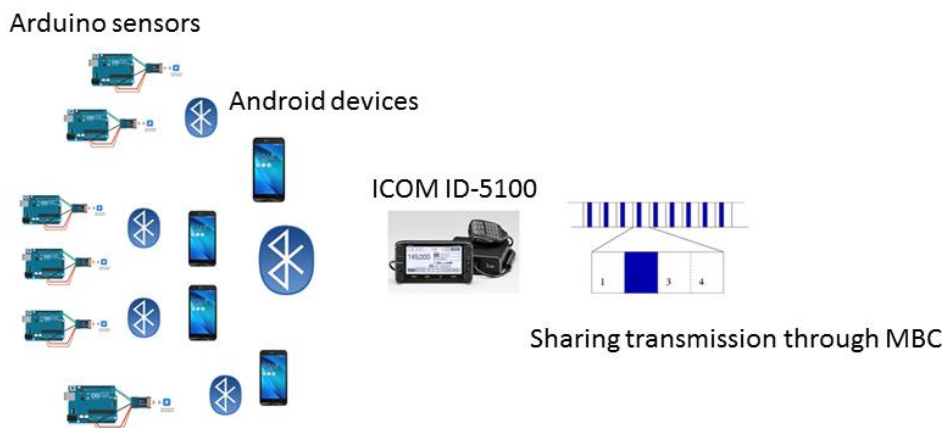


Figure 4.11 Increasing the capacity of the MBC system through Bluetooth pairing.

4.3.6 Modulation

The modulation used in the D-STAR protocol is the Gaussian Minimum Shift Keying (GMSK), which is the same modulation used for the cellular networks due to its bandwidth efficiency. The bandwidth efficiency however does not have a significant impact on the performance of MBC links unless several frequency channels are operating simultaneously. The GMSK modulated signals preserves constant amplitude making them less impacted by noise. The significant consideration on MBC by using this modulation type is the requirement of high SNR to achieve the same bit error rate (BER) level [42]. This could be another trigger for using higher power transmission levels. The GMSK was recommended for meteor scatter systems use in the MBC technical report issued by the European Radiocommunications Committee (ERC) [43], which generally validates its compatibility with MBC.

4.3.7 Reliability

MBC systems are designed following either of two general techniques: 1- The broadcast technique, where the transmitter continuously transmits data bursts blindly in search for a usable meteor trail. This technique is of random nature with less intelligence and is ideal with one-way applications with no data logging. 2- The probing technique, where the transmitter continuously send short probe signals while listening to an acknowledge signal from the receiver. Once an acknowledge signal is received, the data burst transmission starts immediately. The probing technique is the most common among commercial applications due to its added reliability on the expense of using portion of the trail decay time in handshaking. As stated earlier, using the D-STAR repeaters in receiving the meteor scattered bursts through internet allows using the broadcast technique only. The probing technique can be applied in the D-STAR simplex mode in the case of high power at long distances due to the relatively large burst size. The limited meteor trail decay times at short distances and low power may not be sufficient for adding additional handshaking time.

4.4 Experimental setup

A common approach for MBC designers is to use software modeling to predict the system performance while changing several combinations of antenna types, power levels, data rates, protocols and ranges. The result of these predictions identifies whether the MBC link will be an efficient option for the required scenario or not and consequently decides whether to construct a real system or not. Software modeling has several advantages such as minimizing the effort and cost. However, for our case at KUT with an educational scope, achieving an accurate and stable MBC software model would normally require longer time than practical testing specially for the different protocol used of D-STAR network. Also, there were several practical aspects essential to be checked for future end-to-end applications such as the stability of the DV low speed Android application, the Bluetooth pairing performance and the D-STAR routing options. Accordingly, we have chosen to go with a practical simple proof of concept experiment and leave the software modeling as a candidate future work. An obstacle we faced as amateur beginners is the limited power permitted by the basic amateur transmitting license of 20 watts only. Based on the previous analysis, we estimated that this power level will not be sufficient for MBC at the given frequency of 144 MHz. However, as two consecutive large meteor showers were approaching, the Geminids and the Quadrantids, we have decided to proceed with simple testing during the two events. Based on our previous observational records by the KUT meteor radar, during meteor showers the average detection rate of overdense

meteor echoes is 10 per hour during early morning time. Our estimation was that this detection rate level can be degraded to 1 meteor echo per hour for the frequency and power used.

Testing with a D-STAR gateway repeater was the optimum scenario so that we would require only a transmitter, but unfortunately the most recent updated D-STAR repeater map in Japan did not show any repeaters operating at the desired C-band [44]. Also, it was not likely that the complete transmitted bursts can be delivered correctly at the used power level. A simplex scenario between a remote transmitter and a base station receiver at KUT campus was designed. The land terrain nature of Japan was suitable for behind line of sight (BLOS) testing. The presence of high mountains that block the line of sight has allowed testing at short ranges of 100 to 150 km within the Shikoku Island. This short range is considered as a worst case option for MBC as the reflection angle becomes very narrow. Some MBC scientists even assume that short ranges below 200 km can result in a combination of forward and back scattering or totally back scattering (*e.g.* [45]). The short range testing was acceptable for us as a proof of concept experiment so that if a D-STAR burst is successfully received by partial forward scattering then it has a better chance with full forward scattering over longer ranges.

4.4.1 Transmitter

The experimental setup is shown in Fig. 4.12. The transceiver and the lead battery are of minimum size that easily fit in a 30 cm x 40 cm box (Fig. 4.13). The ICOM ID-5100 transceiver was selected with the extra Bluetooth chip UT-133 to allow pairing with Android devices. This should provide more flexibility for larger vehicles such as Trucks or Ships where the Android device can roam freely. The transceiver has a separate flat touch screen that can be placed out of the box for transmission checking if needed. The capacity of the lead battery is sufficient for low speed automatic transmission up to 6-8 hours minimum before it needs recharge. The battery has an interface to solar panel chargers that can be suitable for the sunny desert environment. The transceiver is paired with an Android device ASUS MEMO PAD 7 with the ICOM application RS-MS1A installed. Not all the ICOM transceivers are compatible with the Android application RS-MS1A nor all the Android devices are. The list of compatible devices for both is available on ICOM website and the Google app store. The Android application “MBC Test” was developed locally for testing purpose. The role of the application is to extract the android built-in sensor data and transmit them through the RS-MS1A application using the Android intent features (Fig. 4.14). Thus, the “MBC Test” application acts as a bridge from the sensors to the radio interface application RS-MS1A. The system is designed to follow the broadcast technique with no probing signal nor data logging. The choice of the broadcast technique over the probing technique is based on the limited meteor scattering time expected at the used frequency and power levels. The handshake process can add an additional time of 20-100 ms on average [46]. The intervals between retransmissions are made as short as 5 seconds to ensure that any meteor trails of overdense type are not missed. The specifications of the transmitter are summarized in Table 4.1.

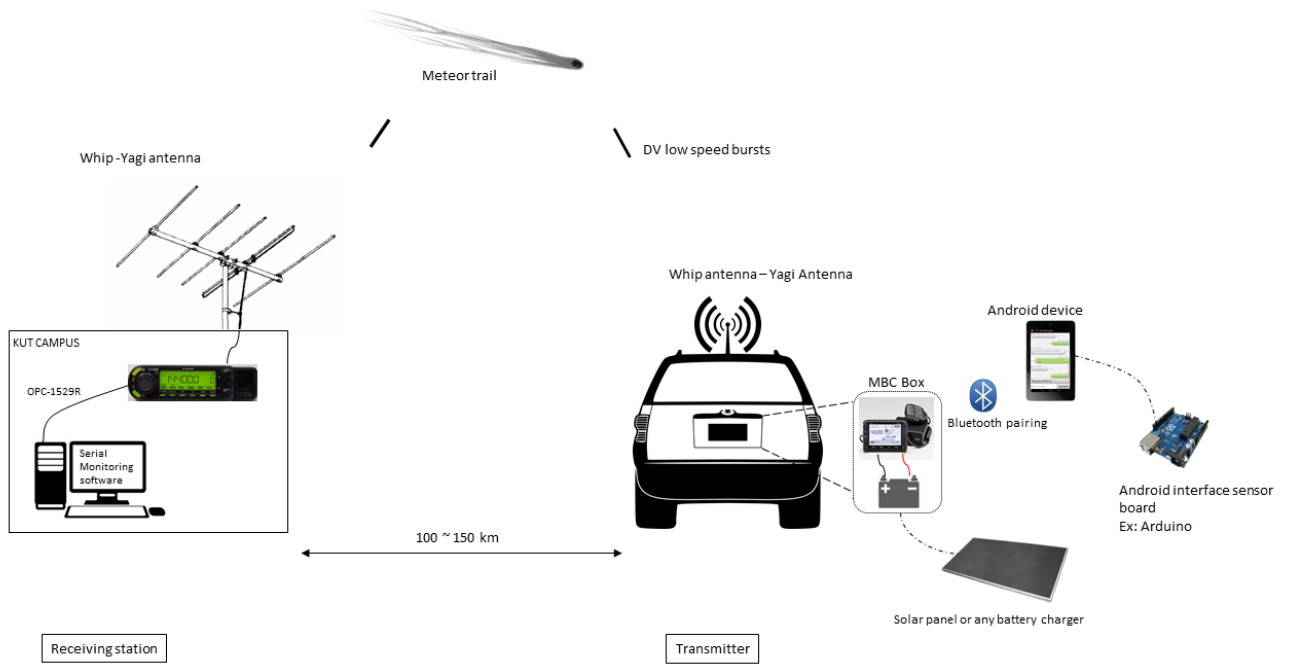


Figure 4.12 Experimental setup.



Figure 4.13 The MBC box.

Table 4.1 Transmitter specifications.

Transceiver	ICOM ID-5100
Frequency	145.250 MHz
Antenna	Vertical whip ¼ wavelength or 5 element Yagi
Bandwidth	6.25 KHz
DV data rate	4800 bps
Transmitting Power	15 W
Power source	Rechargeable Lead battery 12V, 20Ah

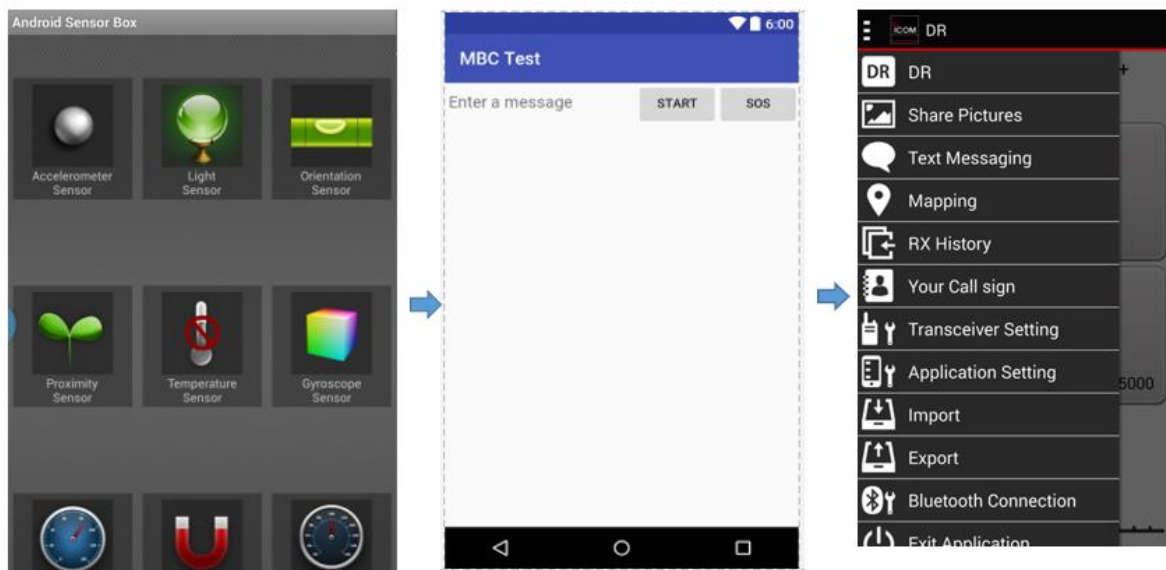


Figure 4.14 The developed MBC Test application and the ICOM RS-MS1A.

4.4.2 Receiver

A receiving station was installed in the meteor observation hut in the KUT campus. The receiver ICOM ID-880H is connected to a windows desktop PC through the serial cable ICOM OPC-1529R. Two free software applications were installed on the PC; 1- The D-RATS software that provides the far-end keyboard application required for low speed serial data communication in the DV mode and 2- A free serial monitoring software “Free Serial Port Monitor” that displays the raw bytes of the data received. The D-RATS software records the received bursts and their time continuously. The serial monitoring software is used to monitor the amount of errors in the received bursts and can be used in extracting data from the partially received bursts in future end-to-end applications. An example is the SOS message sent by the RS-MS1A application in-lab and received by the D-RATS and the serial monitoring software as shown in Fig. 4.15 and Fig. 4.16, respectively.

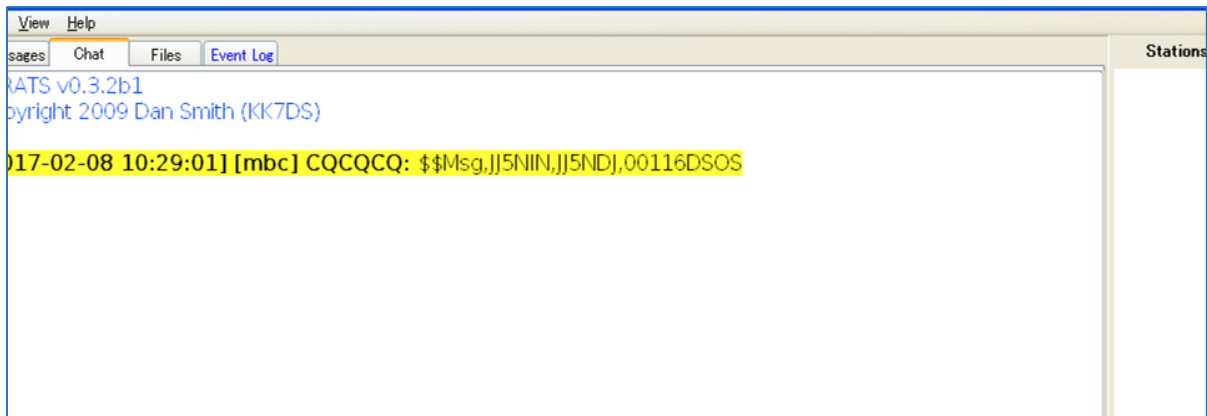


Figure 4.15 SOS message received by the D-RATS software.

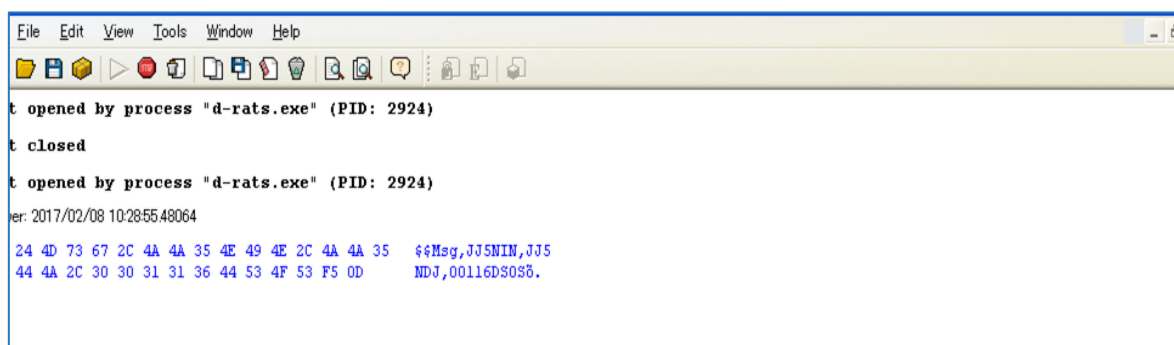


Figure 4.16 SOS message raw data received by the serial monitoring software.

4.5 Testing

The testing plan was divided into sessions of 4 hours each at the early morning time from 3 AM to 7 AM during the peak days of the Geminids 2016 and Quadrantids 2017 meteor showers. The system has no data logging and the existing value of the built-in sensor was planned to be directly transmitted every 5 seconds. The required was to simulate a scenario where a sensor value is transmitted to the receiving station within waiting time intervals of 1 hour maximum. In such applications, the waiting time between successful transmissions becomes the first design priority over the amount of data successfully transmitted throughout a specific period of time. The developed Android software application “MBC Test” responsible for forwarding the sensor value to the transmitter was not yet completely stable due to technical issues while automatic interacting with the commercial ICOM application RS-MS1A. There was a debate by Android developers whether it is feasible to automate transmission through Android intent features or not. As Android developments was out of the wireless compatibility scope, not much focus was given on this part and was postponed to future end-to-end applications. Testing was therefore performed interchangeably by manual transmission through the RS-MS1A application and the transceiver’s built-in GPS NMEA (National Marine Electronics Association) VTG (Vector track and Speed over the Ground) automatic message to test the main wireless part. The VTG message was selected as it is the shortest type of the GPS formats available with burst duration of 950 ms measured in the laboratory.

4.5.1 Geminids 2016

The first test was performed during the Geminids meteor shower on December 14th and 15th using vertical whip $\frac{1}{4}$ wavelength antennas for transmitting and receiving. At that time, Yagi antennas were not yet delivered due to logistic problems and whip antennas were selected for its ease of use with mobile applications. The transmission was from Cape Ashizuri at a distance of 120 km from the receiving station at the KUT campus (Fig. 4.17). Only noise was received and no correct bursts were recognized. This was expected due to the low gain of whip antennas that make it almost impossible to work on an MBC link at this very low power levels. Also, the whip antennas radiation pattern although illuminates larger areas in the sky, has a theoretical null towards the vertical direction where several studies have recommended the presence of a scattering hot spot above the transmitter for short ranges [47]. Initially from (9), the midpoint between the transmitter and the receiver is considered a hotspot due to the position of the maximum reflection angle. This is effective in case of long distances of more than 500-600 km. For shorter distances, the reflection angle impact on performance decreases and the hot spots are shifted to the region above the transmitter and the receiver. As the condition for the forward scattering of radio signals by meteor ionized trails requires that the meteor trails be a tangent to an ellipsoid with the transmitter and receiver at the foci points, the scattering meteor trails above the transmitter has also another advantage of larger foot print illuminated on the receiving side. In Fig. 4.18, the illuminated footprint by tangent meteor trails at 3 directions is shown: 1- area above the transmitter, 2- mid-link area and 3- area above the receiver. It is shown that the meteor trails tangent to the ellipsoid section above the transmitter illuminates larger footprint on the receiver side. The larger footprint in other words means the existence of more valid ellipsoids with the transmitter as one of the foci and a wider range for the other foci around the receiver. Thus any meteor trails that are tangent to these ellipsoids could be usable. As a result, the $\frac{1}{4}$ wavelength vertical whip antennas was not successful to provide a suitable combination for MBC due to several reasons.



Figure 4.17 Initial testing location during the Geminids meteor shower

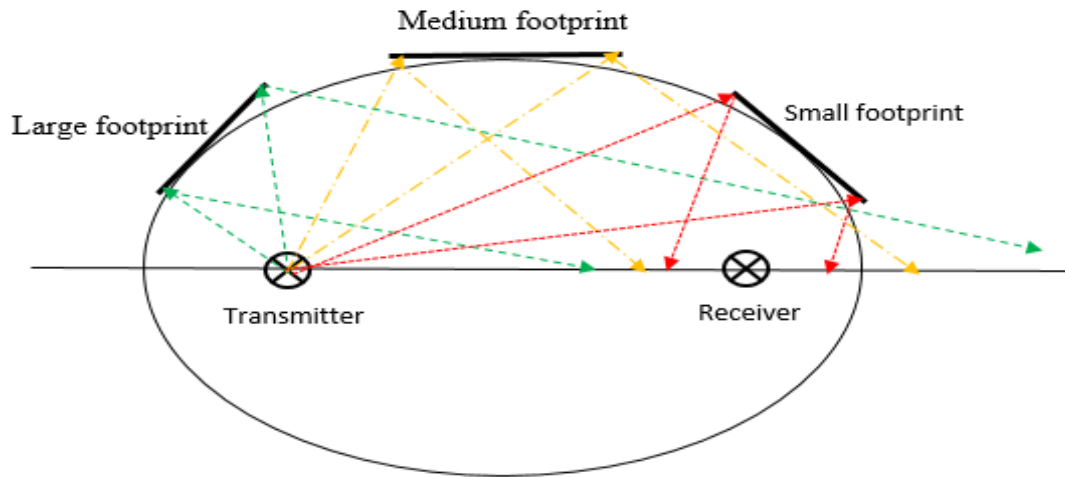


Figure 4.18 Meteor trail locations and the corresponding illuminated ground footprints.

4.5.2 Quadrantids 2017

Directional 5 element Yagi antennas with 9dBi gain were used during the Quadrantids meteor shower testing session on the morning hours of 4th and 5th January 2017. The transmitting antenna at one wavelength height was directed towards the vertical direction above the transmitter. A receiving vertically polarized Yagi antenna at one wavelength height was directed towards the meteor altitude region above the transmitter (90 km average). As the scattered radio signals from the meteor ionized trails is of random nature, we have not considered a preference for vertical or horizontal polarization in the receiving site. From our previous practice with the observational system, the cross polarized receiving antennas show the best performance for meteor scatter, however, this type was not available for the 2 m wavelength at the time of testing.

While configuring the receiver we aimed at eliminating noise by targeting full correct bursts through adjusting the squelch settings to the call sign squelch. This has eliminated noise but still no correct bursts were received. Aiming for full burst reception appeared to be not so wise decision as any partially received bursts must have been filtered. We realized later that the reception of parts of the burst could be usefully interpreted by software scanning of raw data to extract the useful portion of data at the known location at the very end of the burst.

Several testing session were performed after the Quadrantids test targeting sporadic meteors but no useful results were obtained as expected with very low transmitting power level. The time window for testing was almost finished as the nearest major meteor shower will be the Perseids in July 2017.

4.6 Summary

The preliminary analysis on the compatibility of the wireless features of D-STAR for usage with MBC reveals the requirement of high transmitting power over long ranges. As the power sources are normally limited in the rural areas, renewable power sources can be considered such as solar panels or wind turbines. Full burst correct scattering would rely on the meteor trails of the overdense type. Partial scattering by the underdense echoes may work by developing a scanning software for the serial raw data received. Working MBC on D-STAR may fit better with the broadcasting type with no handshaking due to the short trail decay time expected and therefore can be used in backup or emergency systems. Except for the impact of

the high frequency, there is no specific drawback appearing that can prevent using D-STAR for MBC. The concept is although not yet proved, however it is not disproved also. The initial testing was not successful most probably due to the very low power used. Further testing with high transmitting power levels at longer distances to compensate for the high frequency used should be the next necessary step. Antenna design is also another essential component to reach the optimum combination of transmitting and receiving patterns for the most efficient utilization of the available transmitting power. Once the wireless part is confirmed, it will be the Android software developers' call to build interface applications between external sensors and ICOM RS-MS1A application or directly to the radio transceivers.

CHAPTER 5

Conclusion and Future Work

5.1 Summary

The usage of forward scattering of radio signals from the meteor ionized trails in three different applications is presented. The methodology used in each application is described accompanied by sample observations as a proof of concept. The observational results obtained for the meteor astronomy and atmospheric science applications through the developed software system are in agreement with the fundamentals of meteor science in both fields. The advantage of the meteor observation system described is its relative low cost compared to the professional systems. The system overall cost is around eight thousand dollars excluding the transmitter cost at Sabae station. As the ham-band common transmitter in Japan can be a special case, building a transmitting point with the same specifications would add around one thousand dollars to the total cost in addition to the running cost of continuous power transmission. A new branch of meteor study was initiated through a preliminary feasibility study on using the D-STAR ham-band network to add extra flexibility and connectivity options to the MBC systems. Although no positive results were obtained, the potential for using D-STAR for MBC system is worth continuing the research through the proposed approach. The cost of the tools used in the MBC experiment is less than two thousand dollars and can be extended to three thousand dollars for the real long term applications.

5.2 Application overlaps

The three applications described rely on the same concept of radio forward scattering by the meteor ionized trails. This demonstrates that the three research areas are not isolated from each other and several overlapping parameters exist among them. The basic parameters of meteor flux rates, meteor echo durations and meteor echo directions show overlapping importance for the three applications as summarized in Table 5.1. Astronomers performing statistical analysis on meteor flux rates during specific periods of meteor showers or normal days sporadic meteors have to consider the changing atmospheric conditions that might impact the decay time of the meteor ionized trails. The changing conditions of the mesospheric ozone concentration and the solar activity as explained in Chapter 3 is an example of these changes. Other atmospheric conditions impacting meteor flux rates include upper atmospheric wind speed level and upper atmospheric temperature. The estimation of the number of usable meteor ionized trails for MBC should also take the observational statistics into consideration. The observational statistics would be useful in estimating the waiting times between overdense meteor trails characterized by long echo durations. It is one of the objectives of this thesis work to highlight the importance of considering more comprehensive approach while performing meteor research using radio instruments.

Table 5.1 Overlapping parameters among the three applications.

Parameters	Astronomy	Atmospheric Science	MBC
Meteor Flux Rates	<ul style="list-style-type: none"> • Meteor showers activity level. • Sporadic meteors statistics. • Diurnal/Seasonal Variations 	<ul style="list-style-type: none"> • Duration distribution curves for Ozone and solar activity observations 	<ul style="list-style-type: none"> • Rate of usable meteor trails • Waiting time between successful receptions
Meteor Echo Duration	<ul style="list-style-type: none"> • Overdense/underdense meteors. • Meteor mass and velocity. 	<ul style="list-style-type: none"> • Duration distribution curves for Ozone and solar activity observations 	<ul style="list-style-type: none"> • Optimum burst size. • Optimum distance between TX and RX.
Meteor Echo Direction	<ul style="list-style-type: none"> • Meteors trajectory and velocity. • Meteors origin 	<ul style="list-style-type: none"> • Meteor heights. • Ozone concentration vertical profile. 	<ul style="list-style-type: none"> • Hotspot directions. • Footprint size.

5.3 Future work

The specific recommended next steps for the three research areas are mentioned in the summary section at the end of each chapter. The observational results included throughout this thesis are sample results presented as a positive proof of concept to the methodology used. Therefore, larger amounts of observational data are still required for statistical analysis to provide deeper level of scientific details. Also, the link and dependencies between the three applications still require more attention. Future work could also attempt other applications where radio forward scattering by meteor trails can be used. Upper wind speed observations, upper atmospheric temperature measurements or even assessing the risk of meteor shower outbursts on space crafts are some examples of other applications. In parallel to the forward scattering techniques, other low cost instrumentations such as video cameras or infrasound microphones can also be involved as supportive tools.

5.4 Conclusion

The main objective of this thesis work in establishing a comprehensive and practical low cost meteor research system has been achieved to a high degree. Internally, the KUT meteor observation system was mainly constructed for educational purpose and has been run by successive graduate students step by step with their own skills since 2004. This thesis work in turn has built on the previous developments of graduate students at KUT and paved the way for a wider range of possible research work for the upcoming graduate students. On the meteor research worldwide level, the approach of the KUT meteor observation system could be considered as a “gap-filler” between the simple amateur systems and the high-cost professional ones. The meteor astronomy work described in Chapter 2 was introduced in the Meteoroids 2016 conference as one of the top examples of the amateur work efforts in worldwide [48]. As one of the objectives of the meteor observation group at KUT is to provide a model for low-

budget educational institutes worldwide to follow, the recent group publications and conference participations aimed at providing the development experiences required to replicate this work. The developed software applications were also made free for use or enhancements by other groups. There are still however several challenges facing the long run objectives. As being operated by graduate students, the continuity of the system operation can be interrupted by gaps between students' assignments due to lack of students with specific interest in meteor studies. This may cause missing of essential observational data during these gaps and hence rework could be required. It is then recommended to keep overlapping students working on the system without interruptions.

An expected comment by readers of this thesis work would be that the distribution of research efforts among three different research areas might have limited the ability to reach deeper results in each. Such argument can be valid as the narrow vertical approach is the most common among researchers. However, one of the objectives of this thesis work is to provide a wide horizontal insight on the radio forward scattering by meteor ionized trails usability and highlight the links between the different applications as described in Sec. 5.3.

The theme of the thesis varied from radio instrumentation developments to serve scientific research purposes to the other way around of applying scientific information in engineering a practical communication system. Such a balanced approach between science and engineering could be ideal for space research activities where scientists and engineers usually have different perspectives. The thesis work although was carried out from an engineering perspective, however meteor science has been included up to an adequate level.

Bibliography

- [1] Imoto, S., Hasegawa, I., Historical records of meteor showers in China, Korea, and Japan. *Smithsonian contributions to astrophysics*. 2:131, 1958.
- [2] Rehren, T., Belgya, T., Jambon, A., Káli, G., Kasztovszky, Z., Kis, Z., Kovács, I., Maróti, B., Martínón-Torres, M., Miniaci, G. and Pigott, V.C., 5,000 years old Egyptian iron beads made from hammered meteoritic iron. *Journal of Archaeological Science*, **40**(12), pp.4785-4792, 2013.
- [3] Olmsted, D., Observations of the meteors of November 13, 1833, *American Journal of Science* **25**, 354-411, 1834.
- [4] Fairbridge, R. W., SCHIAPARELLI, GV Schiaparelli, Giovanni Virginio (1835–1910), *Encyclopedia of Planetary Science*, 725-726, 1997.
- [5] Trowbridge, C. C., Physical nature of meteor trains, *The Astrophysical Journal*, **26**, 95, 1907.
- [6] Öpik, E. J., A statistical method of counting shooting stars and its application to the Perseid shower of 1920, *Observatoire astronomique de l'Université de Tartu (Dorpat)*, 1922.
- [7] Breit, G., and Tuve, M. A., A test of the existence of the conducting layer, *Phys. Rev.*, **28**, 554-573, 1926.
- [8] Nagaoka, H., Possibility of disturbance of radio transmissions by meteoric showers, *Proceedings of the Imperial Academy, Tokyo*, 5:233, 1929.
- [9] Adams, J.H., Ahmad, S., Albert, J.N., Allard, D., Anchordoqui, L., Andreev, V., Anzalone, A., Arai, Y., Asano, K., Pernas, M.A. and Baragatti, P., JEM-EUSO: Meteor and nuclearite observations, *Experimental Astronomy*, **40**(1), pp.253-279, 2015.
- [10] McKinley, D.W.R., Meteor Science and Engineering, McGraw-Hill, New York, 1961.
- [11] Murad, E., and Williams, I. P., Meteors in the Earth's Atmosphere: Meteoroids and Cosmic Dust and Their Interactions with the Earth's Upper Atmosphere, Cambridge University Press, 2002.
- [12] Ceplecha, Z., Borovička, J., Elford, W.G., ReVelle, D.O., Hawkes, R.L., Porubčan, V., Šimek, M., Meteor phenomena and bodies, *Space Sci. Rev*, **84**(3–4), 327–471, 1998.
- [13] DeMeo, F. E., C. M. O. D. Alexander, K. J. Walsh, C. R. Chapman, and R. P. Binzel, The Compositional Structure of the Asteroid Belt, *Asteroids IV*, **1**, 13, 2015.
- [14] Janches, D., S. E. Palo, E. M. Lau, S. K. Avery, J. P. Avery, S. de la Pena, and N. A. Makar, Diurnal and seasonal variability of the meteoric flux at the South Pole measured with radars." *Geophysical research letters* **31**, no. 20, 2004.

- [15] National Research Council. Limiting Future Collision Risk to Spacecraft: An Assessment of NASA's Meteoroid and Orbital Debris Programs. National Academies Press, 2011.
- [16] Meteoroids conference 2016 Program, <https://www.cosmos.esa.int/web/meteoroids2016/conference-programme> Accessed March, 2017.
- [17] Higa, Y., Yamamoto, M-Y., Toda, M., Maeda, K. and Watanabe, J-I, Catalogue of persistent trains II: images of Leonid meteor trains during the METRO campaign 1998-2002, *Publications of the National Astronomical Observatory of Japan*, **7**, pp.67-131, 2005.
- [18] Maegawa, K.: HRO: a new forward-scatter observation method using ham-band beacon. *WGN* **27**, 64–72, 1999.
- [19] Ranvier, S., H. Lamy, M. Anciaux, S. Calders, E. Gamby, and J. De Keyser. Instrumentation of the Belgian radio meteor stations (BRAMS), 2015 International Conference on Electromagnetics in Advanced Applications (ICEAA), pp. 1345-1348. IEEE, 2015.
- [20] Jones, J., Webster, A.R., Hocking, W.K., An improved interferometer design for use with meteor radars. *Radio Sci.*, **33**, 55–65, 1998.
- [21] Noguchi, K., Yamamoto, M.-Y.: Development of an automatic echo-counting program for HROFFT spectrogram. *Earth Moon Planet*, **102**, 323–329, 2008.
- [22] Weryk, R.J., Brown, P., A search for interstellar meteoroids using the Canadian meteor orbit radar (CMOR), *Earth Moon Planet*, **95**, 221–227, 2005.
- [23] Kaiser, T.R., Radio echo studies of meteor ionization, *Adv. Phys.*, **2** (8), 495–544, 1953.
- [24] Davis, J.A., Greenhow, J.S., Hall, J.E., The effect of attachment on radio echo observations of meteors, *Proc. R. Soc. Lond. Ser. A, Math. Phys. Sci.*, **253**(1272), 130–139, 1959.
- [25] Baggaley, W.J., Cummack, C.H., Meteor train ion chemistry, *J. Atmos. Terr. Phys.*, **36**, 1759, 1974.
- [26] Baggaley, W.J., The interpretation of overdense radio meteor echo duration characteristics, *Bull. Astron. Inst. Czechoslov*, **30**, 184–189, 1979.
- [27] Jones, J., McIntosh, B.A., Simek, M., Ozone and the duration of overdense radio meteors, *J. Atmos. Terr. Phys.*, **52**(4), 253–258, 1990.
- [28] Merkel, A.W., Harder, J.W., Marsh, D.R., Smith, A.K., Fontenla, J.M., Woods, T.N., The impact of solar spectral irradiance variability on middle atmospheric ozone. *Geophys. Res. Lett.*, **38**, L13802, 2011.
- [29] Forsyth, P.A., Vogan, E.L., Forward scattering of radio waves by meteor trails. *Can. J. Phys.*, **33**(5), 176–188, 1955.

- [30] Carbognani, A., De Meyere, M., Foschini, L., Steyaert, C., On the meteor height from forward scatter radio observations, *Astron. Astrophys.*, **361**, 293, 2001.
- [31] Jacchia, L.G., Verniani, F., Briggs, R.E., Selected results from precision-reduced super-Schmidtmeteors, *Smithson. Contrib. Astrophys.*, **11**, 1, 1967.
- [32] Neslusan, L.: A summary of the research of Geminid meteoroid stream. *Contrib. Astron. Obs. Skaln. Pleso*, **45**, 60–82, 2015.
- [33] Smith, A.K., Harvey, V.L., Mlynczak, M.G., Funke, B., García-Comas, M., Hervig, M., et al.: Satellite observations of ozone in the upper mesosphere, *J. Geophys. Res., Atmos.*, **118**, 1–19, 2013.
- [34] Forsyth, P. A., E. L. Vogan, D. R. Hansen, and C. O. Hines, The principles of JANET-A meteor-burst communication system, *Proceedings of the IRE 45*, no. **12**, 1642-1657, 1957.
- [35] Bartholome, P., and I. Vogt, COMET--A New Meteor-Burst System Incorporating ARQ and Diversity Reception, *IEEE Transactions on Communication Technology* **16**, no. **2**, 268-278, 1968.
- [36] Johnson, D. E., Ten years experience with the SNOTEL meteor burst data acquisition system, *In Proc. Meteor Burst Commun. Symp.* The Hague, Netherlands, Nov. 1987, vol. **5**. SII-5-SII-20, 1987.
- [37] Fukuda, A., Kaiji, M., Yasuaki, Y., Masauji, N., Hisao, Y., Natsuo, S., Huigen, Y., Ming, W.Y., and Li, J.J., Experiments on meteor burst communications in the Antarctic, *Advances in polar upper atmosphere research* **17**, 120-136, 2003.
- [38] Charania, A., Networks on the Edge of Forever: Examining the Feasibility of using Meteor Burst (MB) Communication Networks on Mars, *In IAF abstracts*, 34th COSPAR Scientific Assembly. 2002.
- [39] Baggaley, W. J., and G. W. Fisher, Measurements of the initial radii of the ionization columns of bright meteors, *Planetary and Space Science* **28**, no. **6**, 575-580, 1980.
- [40] Schilling, Donald L., ed. Meteor burst communications theory and practice, Vol. **24**. Wiley-Interscience, 1993.
- [41] Murota, Kazuaki, and Kenkichi Hirade, GMSK modulation for digital mobile radio telephony, *IEEE Transactions on communications* **29**, no. **7**, 1044-1050, 1981.
- [42] Dual band transceiver ID-5100A, service manual, ICOM Inc., 2016.
- [43] Meteor Scatter Applications, European Radiocommunications Committee (ERC) within the European Conference of Postal and Telecommunications Administrations (CEPT), Vilnius, June 2000.

- [44] Japan D-STAR Repeater Map (In Japanese), Nagoya Digital Communication Conference 2016, Available: <http://isotope.sist.chukyo-u.ac.jp/dstar2/IntroductiontoD-STARforPrint.pdf>, Accessed on Dec. 2016.
- [45] Abel, M., Meteor burst communications, Bits per burst performance bounds, *IEEE transactions on communications* 34, no. **9**, 927-936, 1986.
- [46] Yavuz, D., Meteor burst communications, *IEEE Communications Magazine* 28, no. **9**, 40-48, 1990.
- [47] Weitzen, J. A. Y. A., Communicating via meteor burst at short ranges, *IEEE transactions on communications* 35, no. **11**, 1217-1221, 1987.
- [48] Rendtel, J.: Amateur Meteor Work, Meteoroids conference (2016).
- [49] Madkour, W., and Yamamoto, M-Y., Mesospheric observations by a forward scattering meteor radar basic setup, *Astrophys Space Sci*, 361: 247, 2016.
- [50] Madkour, W., Yamamoto, M.-Y., Kakinami, Y., Mizumoto, S.: A low cost meteor observation system using radio forward scattering and the interferometry technique. *Exp. Astron.*, **41**, 243–257, 2016.
- [51] D-STAR System, Japanese Amateur-Radio League (JARL) <https://www.jarl.com/d-star/shogen.pdf> , Accessed on Feb. 2017.

Appendix A

Meteor echo direction radio/optical simultaneous observations

Table A.1 Simultaneous observation results by the interferometer (shaded rows) and video cameras (white rows) for the north-west direction (first camera FOV)

DATE YYYYMMDD	DETECTIO N TIME[LT]	AZIMUT ANGLE [DEG]	ELEVATION ANGLE [DEG]	DURATION [S]	INTENSITY [0-12] [A.U.]
20090103	23:23:50	351	35	1	12
	23:23:50	345	36		
20090104	01:29:33	338	38	10	12
	01:29:33	346	42		
20090104	02:17:40	340	35	15	12
	02:12:37	341	34		
20090104	03:00:11	350	44	12	12
	03:00:10	349	44		
20090104	03:21:04	348	45	1	12
	03:21:04	344	47		
20090104	03:27:46	350	37	11	12
	03:27:44	350	39		
20090104	03:35:22	331	33	4	12
	03:35:23	336	37		
20090104	03:36:21	341	34	10	12
	03:36:21	340	35		
20090104	03:46:03	334	34	13	12
	03:46:03	331	34		
20090104	04:30:22	356	64	4	12
	04:30:22	352	64		
20090104	04:49:02	352	35	5	12
	04:48:58	349	33		
20090104	04:58:11	166	51	1	8
	04:58:10	359	23		
20090104	04:59:54	311	69	5	12
	04:59:50	330	45		
20090104	05:04:07	343	25	1	12
	05:04:04	329	57		

20090104	05:16:44	308	57	11	12	(4)
	05:16:44	328	28			
20090104	05:23:22	68	14	1	9	
	05:23:21	0	33			
20090104	05:29:57	176	51	1	10	
	05:29:58	24	44			
20090127	05:57:21	301	54	8	10	
	05:57:17	300	55			
20090127	21:13:22	307	50	4	12	
	21:13:22	303	47			
20090128	00:50:58	248	75	1	9	
	00:50:56	260	45			
20090128	04:15:06	311	50	5	10	
	04:15:02	309	49			
20090128	04:44:33	304	63	5	12	
	04:44:33	303	63			
20090129	04:29:46	330	38	2	12	
	04:29:46	327	34			
20090201	03:39:48	302	52	8	12	
	03:39:47	298	48			
20090202	00:55:03	290	33	1	12	
	00:55:01	255	31			
20090203	03:57:48	286	33	11	12	
	03:57:48	278	29			
20090212	02:34:29	295	52	16	12	
	02:34:25	288	52			

Table A.2 Simultaneous observation results by the interferometer (shaded rows) and video camera (white rows) for the south-east direction (second camera FOV).

DATE YYYYMMDD	DETECTION TIME [LT]	AZIMUTH ANGLE [DEG]	ELEVATION ANGLE [DEG]	DURATION [S]	INTENSITY [0-12] [A.U.]	
20090104	02:20:55	133	49	21	12	(1)
	02:20:54	100	65			
20090104	02:26:42	253	32	3	12	
	02:26:42	99	40			
20090104	03:04:49	142	17	1	8	
	03:04:44	145	69			
20090104	03:54:30	162	18	10	12	(2)
	03:54:30	160	54			
20090104	03:59:05	145	64	1	8	
	03:59:08	98	41			
20090104	04:01:41	119	50	3	12	
	04:01:41	158	70			
20090104	04:24:29	57	66	3	8	
	04:24:33	116	69			
20090104	05:13:26	317	79	3	12	
	05:13:26	160	50			
20090125	02:23:09	163	39	5	12	
	02:23:06	168	38			
20090128	22:11:39	134	55	3	9	
	22:11:36	130	57			
20090129	02:53:50	267	72	1	8	
	02:53:54	138	45			
20090202	04:25:15	313	61	1	9	
	04:25:18	161	54			
20090204	02:43:56	181	45	1	7	
	02:43:56	184	47			
20090204	03:20:57	25	51	1	6	
	03:20:57	159	26			
20090211	21:21:26	180	44	4	12	
	21:21:26	186	42			

Appendix B

Selected technical specifications of the D-STAR wireless system

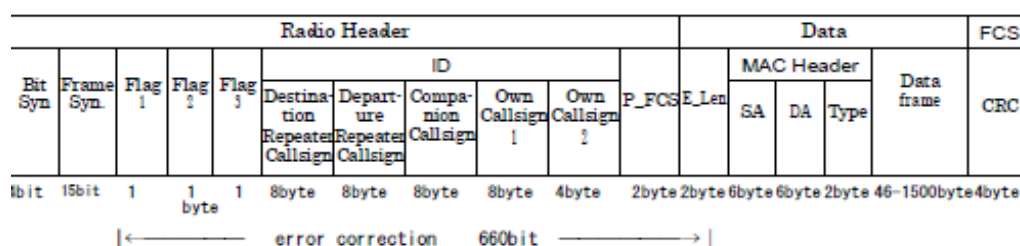
The following is copied from the official English version of the D-STAR technical document by JARL [51]:

2. System Interconnection Requirements

2.1 Wireless Communication Packet

The frame structure of the wireless packet is below.

2.1.1 Frame structure of a data packet



The explanation of the data frame structure the Radio Header follows.

- (1) **Bit Syn.** (Bit synchronization): Repeated standard 64-bit synchronization pattern (for GMSK 1010, for QPSK 1001). Transmission direction is from left to right.
- (2) **Frame Syn.** (Frame synchronization) : 15bit pattern (111011001010000). Transmission direction is from left to right.
- (3) **Flag 1** (8 bit): Flag 1 uses upper 5 bits and lower 3 bits separately. A detailed explanation follows.

bit 7(MSB)	Distinguishes between voice and data communications. 1 indicates data, 0 indicates voice.
bit 6	Identifies if the signal goes through a repeater or is a direct communication between terminals.(1for repeater, 0 for terminal)
bit 5	Recognizes if communication interruption exists. 1 indicates interruption, 0 indicates no interruption.
bit 4	Identifies control signal/data signal.1 represents control signal and 0 represents regular data signal.(Voice signal included)
bit 3	1 represents an urgent priority signal,0 represents a normal priority signal. For signals with a "1" in this position, the receiver will open squelch etc.
Note, Urgent signal in this document does not mean "Urgency signal" as defined in International Radio Law. It means an urgent priority signal for use in emergency communications.	

bit 2,1,0 111=repeater station control flag, while the repeater is controlled, the flag is "111" and the data frame contains control data.

- 110=Auto reply
- 101=Unused(spare)
- 100=Resend flag, requests resending previous frame
- 011=ACK flag, Treated as ACK flag
- 010=No reply flag, Indicates no reply is available
- 001=Relay unavailable flag, Indicates unsuitable relaying conditions.
- 000=NULL, No information.

Upper bit					
Bit	7	6	5	4	3
1	Data	Relay	Interruption	Control	Urgent
0	Voice	Direct	No interruption	Control	Urgent

Lower bit				
2	1	0	Function	Note
1	1	1	Repeater Control	Repeater Control Mode
1	1	0	Auto Reply	Used for Auto Reply
1	0	1	(Unused)	(Unused0)
1	0	0	Resend	Requests Resend
0	1	1	ACK	ACK flag
0	1	0	No Response	Indicates No Response Available
0	0	1	Relay Unavailable	Indicates Relay Unavailable
0	0	0	NULL	NULL

(4) Flag 2

Flag 2 is for future expandability and is defined below.

Bit	7	6	5	4	3	2	1	0	Note
Flag	I D				M				Default
	(0 0 0 0 h)				(* * * * h)				

- a. I D flag is used as an format descriptor. This is available not only for the increase and decrease of a figure of callsign but also for ID, which is not used as callsign rather than numeric.
- b. M flag is used only a creator or a manufacturer of the equipment.

(5) Flag 3

Flag 3 is used to match control functions to protocol versions, which may be upgraded in future software versions.

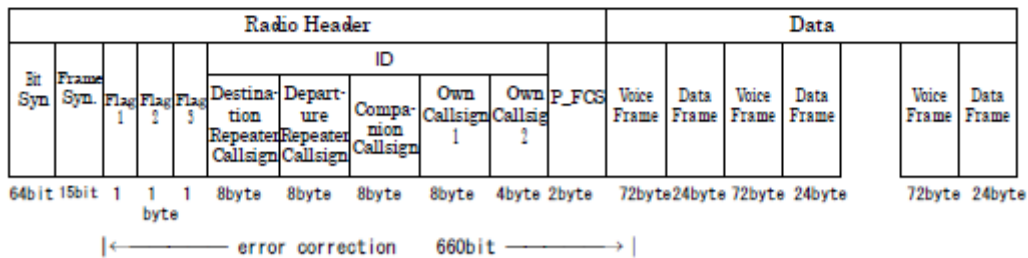
Bit	Meaning	Function
00000000	No Function	Default
00000001	Undefined	Use for future expansion
to		
11111111		

- (6) "Destination repeater Callsign" can have a maximum of 8 ASCII letters and numbers. Blanks should be filled with a space character. In the case of direct communication, it inserts "D I R E C T" and fills the blanks with a space character. The use of this field is described in section 2.2.
- (7) "Departure repeater Callsign" can have a maximum of 8 ASCII letters and numbers. Blanks should be filled with a space character. In the case of direct communication, it inserts "D I R E C T" and fills the blanks with a space character. The use of this field is described in section 2.2.
- (8) "Companion Callsign" can have a maximum of 8 ASCII letters and numbers. Blanks should be filled with a space character. The use of this field is described in section 2.2.
- (9) "Own Callsign 1" can have a maximum of 8 ASCII letters and numbers. Blanks should be filled with a space character. This field same as voice frames.
- (10) "Own Callsign 2" is used when to add suffixes to a callsign or a additional destination address information. "Own Callsign 2" can have a maximum of 4 ASCII letters and numbers. Blanks should be filled with a space character.
- (11) P_FCS is the Radio Header CRC-CCITT checksum, computed by the following expression.

$$G(x) = x^{16} + x^{12} + x^5 + 1$$
- (12) The data frame of the packet is constructed as an Ethernet packet.
- (13) FCS is the checksum of the Ethernet data payload. It is a CRC-32 checksum as defined in ISO3309 and is computed by the following expression.

$$G(x) = x^{32} + x^{26} + x^{23} + x^{22} + x^{16} + x^{12} + x^{11} + x^{10} + x^8 + x^7 + x^5 + x^4 + x^2 + x + 1$$

2.1.2 Frame structure of voice packet



The explanation of the voice packet including the voice and data frames follows:

- (1) The Radio Header has the same frame structure as for the data packet.

- (2) Data part includes 72-bit voice signal frames with a length of 20ms in order of their output from the CODEC according to the AMBE (w/FEC) specification. Data frames contain 24-bits of data.
- (3) The first data frame and then every 21st data frame in a repeating cycle, are used only for synchronizing data for each modulation type. Synchronization corrects for the lag between transmission and reception, including the transit time of communications. This synchronized signal contains a 10-bit synchronized signals and two 7-bit Maximal-length sequences "1101000" patterns. (24 bits total). Transmission direction is from left to right.
- (4) The data in a data frame is transmitted without modification from the input data. If the data is required as error correction or synchronization, these frames are processed before processing the data input.
- (5) If the data signal length is greater than the length of the voice communication the transmitting switch is turned on until the completion of the data signal manually. The processing can be allowed automatically.
- (6) The last data frame, which requires a means of terminating the transmission, is a unique synchronizing signal (32 bit + 15bit "000100110101111" + "0", making 48 bits) as defined by the modulation type. Transmission direction is from left to right.

2.2 Communication protocol

Note : In the following descriptions, _ (under-bar) indicates a space character, ASCII \$20. If the callsign field has blanks between the callsign's last letter and last character in the field, the blanks should be filled with a space character.

2.2.1 Callsign

The Callsign field of the radio header of data and voice packets is used for packet routing. Except for the callsign in the "Own station" fields, callsigns generally have less than 6 letters (or 7 letters). The following paragraphs show how to interpret callsign fields:

(1) "Destination repeater Callsign"

In zone communication, this field must be set to the callsign of the repeater utilized by the companion station.

If there are multiple repeaters in a repeater site, they are distinguished by last character, of "A", "B", "C", or "D". (Ex. W\$1AAA_A , W\$1AAA_D, etc.) The default character is "A".

(Explained callsign is not to exist as W\$1AAA but only for examples)

When communicating outside the local zone, which is called zone to zone communication, this field must be set to the callsign of the zone repeater connected to a gateway and last character set to "G" to indicate communications via the gateway. (Ex. W\$1AAA_G)

(2) "Departure repeater Callsign"

- This field must be set to the repeater callsign of the originating station.
- If there are multiple repeaters in a repeater site, they are distinguished by last character of "A", "B", "C", or "D". (Ex. W\$1AAA_A, W\$1AAA_D etc.) The default character is "A".

(3) "Companion Callsign"

- The field must be set the callsign of the companion station with which communication is desired. If the station has multiple radios,, they are distinguished by last character of "A", "B", "C", "D", "E", or "F". (Ex. W\$1AAA_A, W\$1AAA_F etc.)
- When originating a non-directed call,, the field should contain "CQCQCQ".
- When calling CQ to a non-local zone, which is called zone to zone communication, prepend "/" to the destination repeater callsign. If there are multiple repeaters in a repeater site, they are distinguished by last character of "A", "B", "C", or "D". (Ex. W\$1AAA_A, W\$1AAA_D etc.) The default character is "A".
- To access a repeater with a local server, in "Companion Callsign", the field should contain the repeater callsign and set last character to "S". (Ex. W\$1BBB_S)

(4) "Own Callsign 1"

- The "Own Callsign" field contains the own station's callsign. If the station has multiple radios, they are distinguished by last character of "A", "B", "C", "D", "E", or "F". (Ex. W\$1AAA_A, W\$1AAA_F etc.)

(5) "Own Callsign 2"

This field contains information to display as in after a "/" (slash)". (Ex. W\$1AAA_F / JD1 etc. Note: "/" is not displayed). The purpose of "Own Callsign 2" is to allow "Own Callsign 1" to contain as complete a callsign as possible. "Own Callsign 2" is not evaluated by the system's identification functions.